

# Targeting RECQL5 Functions, by a Small Molecule, Selectively Kills Breast Cancer *in Vitro* and *in Vivo*

Saikat Chakraborty, Kartik Dutta, Pooja Gupta, Anubrata Das, Amit Das, Sunil Kumar Ghosh,\* and Birija Sankar Patro\*

Cite This: *J. Med. Chem.* 2021, 64, 1524–1544

Read Online

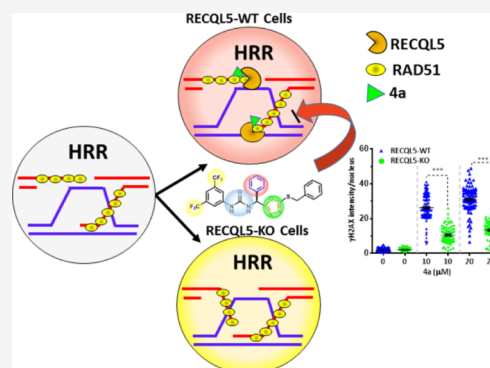
ACCESS |

Metrics & More

Article Recommendations

Supporting Information

**ABSTRACT:** Clinical and preclinical data reveal that RECQL5 protein overexpression in breast cancer was strongly correlated with poor prognosis, survival, and therapeutic resistance. In the current investigation, we report design, synthesis, and specificity of a small molecule, **4a**, which can preferentially kill RECQL5-expressing breast cancers but not RECQL5 knockout. Our stringent analysis showed that compound **4a** specifically sensitizes RECQL5-expressing cancers, while it did not have any effect on other members of DNA RECQL-helicases. Integrated approaches of organic synthesis, biochemical, *in silico* molecular simulation, knockouts, functional mutation, and rescue experiments showed that **4a** potently inhibits RECQL5-helicase activity and stabilizes RECQL5-RAD51 physical interaction, leading to impaired HRR and preferential killing of RECQL5-expressing breast cancer. Moreover, **4a** treatment led to the efficient sensitization of cisplatin-resistant breast cancers but not normal mammary epithelial cells. Pharmacologically, compound **4a** was orally effective in reducing the growth of RECQL5-expressing breast tumors (human xenograft) in NUDE-mice with no appreciable toxicity to the vital organs.



## INTRODUCTION

Breast cancer has presently afflicted 2.1 million females globally<sup>1</sup> and considered as a leading cause of cancer death in women. A better understanding of tumor biology and genomics, development of improved and sensitive diagnostics, and effective and targeted therapeutics have been associated with a reduction of breast cancer patient mortality.<sup>2</sup> Several neoadjuvant/adjuvant chemotherapeutics (cisplatin, doxorubicin, paclitaxel, 5-FU, gemcitabine *etc.*), which causes extensive DNA damages, show positive therapeutic outcomes for breast cancer patients. Besides, targeted chemotherapeutics, like tamoxifen and PARP inhibitors, are successfully used against hormone receptor positive and BRCA1/2 mutated breast cancer patients, respectively.<sup>3–5</sup> However, chemoresistance remains a paramount challenge in the treatment of breast cancer.<sup>3</sup> The presently available interventions are inadequate to target chemoresistance and pathogenesis of breast cancer in patients. To expand the horizon of targeted oncotherapy and clinical medicines, the development of specific drugs for targeting novel key players in breast cancer pathogenesis and *de novo* and/or acquired chemoresistance is urgently required.

RECQL5 is a key member of the human RECQ helicase family. Several lines of evidence suggested that RECQL5 deficiency is associated with genomic instability and development of different types of cancers, including breast cancers.<sup>6,7</sup> On the other hand, high expression of RECQL5, in established

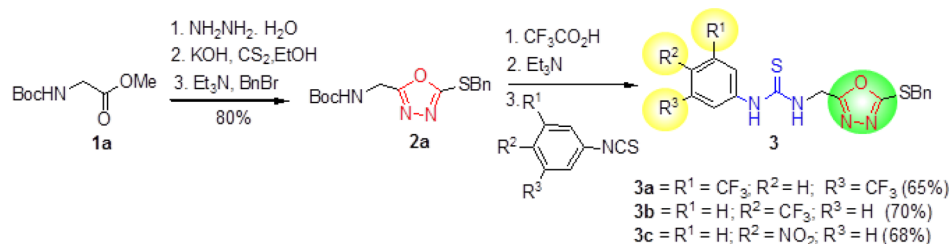
tumors, may promote proliferation and survival of cancer cells. RECQL5 polymorphism is associated with predisposition to laryngeal carcinoma, osteosarcoma, and breast carcinoma.<sup>8–11</sup> Recently, Arora *et al.*, analyzed 1902 breast cancer patients [Nottingham Tenovus series ( $n = 1650$ ) and ER-cohort ( $n = 252$ )] and found that high RECQL5 and low RAD51 protein expressions were significantly linked to high histopathological grade ( $p < 0.0001$ ), higher mitotic index ( $p = 0.008$ ), dedifferentiation ( $p = 0.025$ ), pleomorphism ( $p = 0.027$ ), and poor survival ( $p = 0.003$ ).<sup>12</sup> It has also been found that 53.7% (644/1200) of breast tumors showed a higher expression of RECQL5 in the nucleus. RECQL5 is known to play key roles in homologous recombination, transcription, replication, and other DNA repair process. RECQL5 disrupts RAD51 presynaptic filament by interacting directly with RAD51.<sup>13,14</sup> Interestingly, RECQL5 expression is linked to *de novo* resistance to cisplatin in different types of cancers,<sup>15,16</sup> suggesting a DNA repair role of RECQL5 behind the resistance. Considering its putative role in breast cancer

Received: September 28, 2020

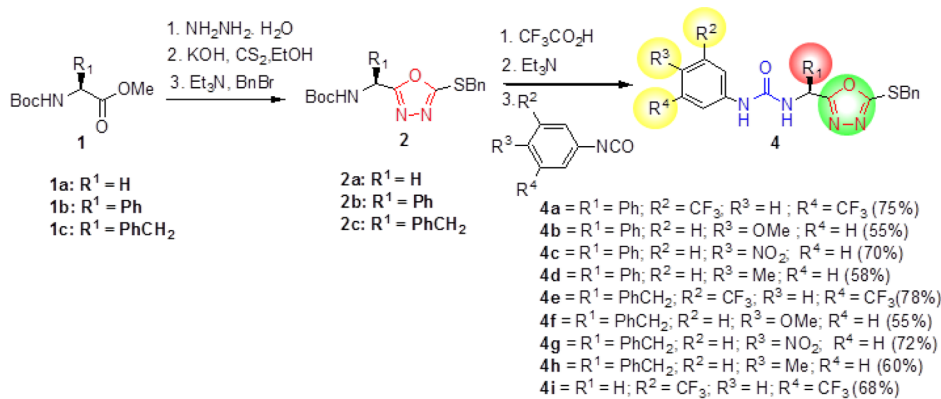
Published: February 2, 2021



Scheme 1. Schematic Routes for the Synthesis of 1,3,4-Oxadiazole with Thiourea Derivatives



Scheme 2. Schematic Routes for the Synthesis of 1,3,4-Oxadiazole with Urea Derivatives



pathogenesis and chemotherapeutics resistance, we hypothesized that targeting RECQL5 with a small molecule may be a key strategy to (1) sensitize RECQL5-expressing breast cancers and (2) abrogate the neoadjuvant/adjuvant-mediated chemoresistance in breast cancer.

Because, the exact molecular function of RECQL5 in breast cancer pathogenesis and chemoresistance is not yet known, we followed a cell-based screening approach to evaluate the potential of small molecule and, designed and synthesized 1,3,4-oxadiazole derivatives in-house, which may preferentially kill RECQL5-expressing breast cancer than RECQL5-deficient breast cancers. Following this approach, we found a small molecule (1-(3,5-bis(trifluoromethyl)phenyl)-3-((S)-(S)-(benzylthio)-1,3,4-oxadiazol-2-yl)(phenyl)methyl)urea, which can preferentially kill RECQL5-expressing breast cancers *in vitro* and is also orally effective in the preclinical breast tumor model. Mechanistically, this small molecule targeted the nonenzymatic domain of RECQL5, stabilized RECQL5-RAD51 physical interaction, and impaired homologous recombinational repair (HRR), which led to the robust sensitization of RECQL5-expressing breast cancer cells. Interestingly, this functional inhibitor of RECQL5 abrogated *de novo* and acquired cisplatin resistance in breast cancers.

## RESULTS

**Chemistry.** *Synthesis of 1,3,4-Oxadiazole Derivatives.* The synthesis pathway for the 1,3,4 oxadiazole thiourea derivatives (compound 3a–3c) is shown in Scheme 1. The

synthesis started with *N*-Boc-protected glycine methyl ester **1a**, which was converted to oxadiazole **2a** following conventional chemical reactions. The *N*-Boc deprotection followed by the reaction with substituted phenylisothiocyanates provided thiourea-substituted oxadiazole derivatives **3a–c** in moderate to good yields. By employing similar reaction sequences, oxadiazole **2b,c** were prepared from appropriate (*S*)-phenylglycine and (*S*)-phenylalanine derivatives, respectively, as shown in Scheme 2. The *N*-Boc deprotection followed by the reaction with substituted phenylisocyanates provided urea-substituted oxadiazole derivatives **4a–i**.

**Biological Evaluation.** *Potential of 1,3,4-Oxadiazole Derivatives to Kill Cancer Cells by Targeting RECQL5.* By analyzing a breast cancer database,<sup>17</sup> comprising 65 patients, we found that the high expression of RECQL5 was inversely associated with overall survival (Figure 1A). Moreover, the exogenous expression of RECQL5 in MCF10A normal breast epithelial cell drives proliferation.<sup>12</sup> Together, these suggest a RECQL5-mediated oncogenic shift in breast cancer cells *in vitro* and in patients. To this end, we asked whether specific pharmacological inhibition of RECQL5 functions may sensitize the breast cancer cells for a better therapeutic outcome. Initially, we screened our in-house small molecule library to find a molecule, which can preferentially kill RECQL5-expressing cells over RECQL5 knockout cells. In order to generate RECQL5-KO cells, control and two different sets of the RECQL5 CRISPR-CAS9 double nickase system were used in MCF-7 cells (ER+/PR+/HER2-, p53 WT). Both

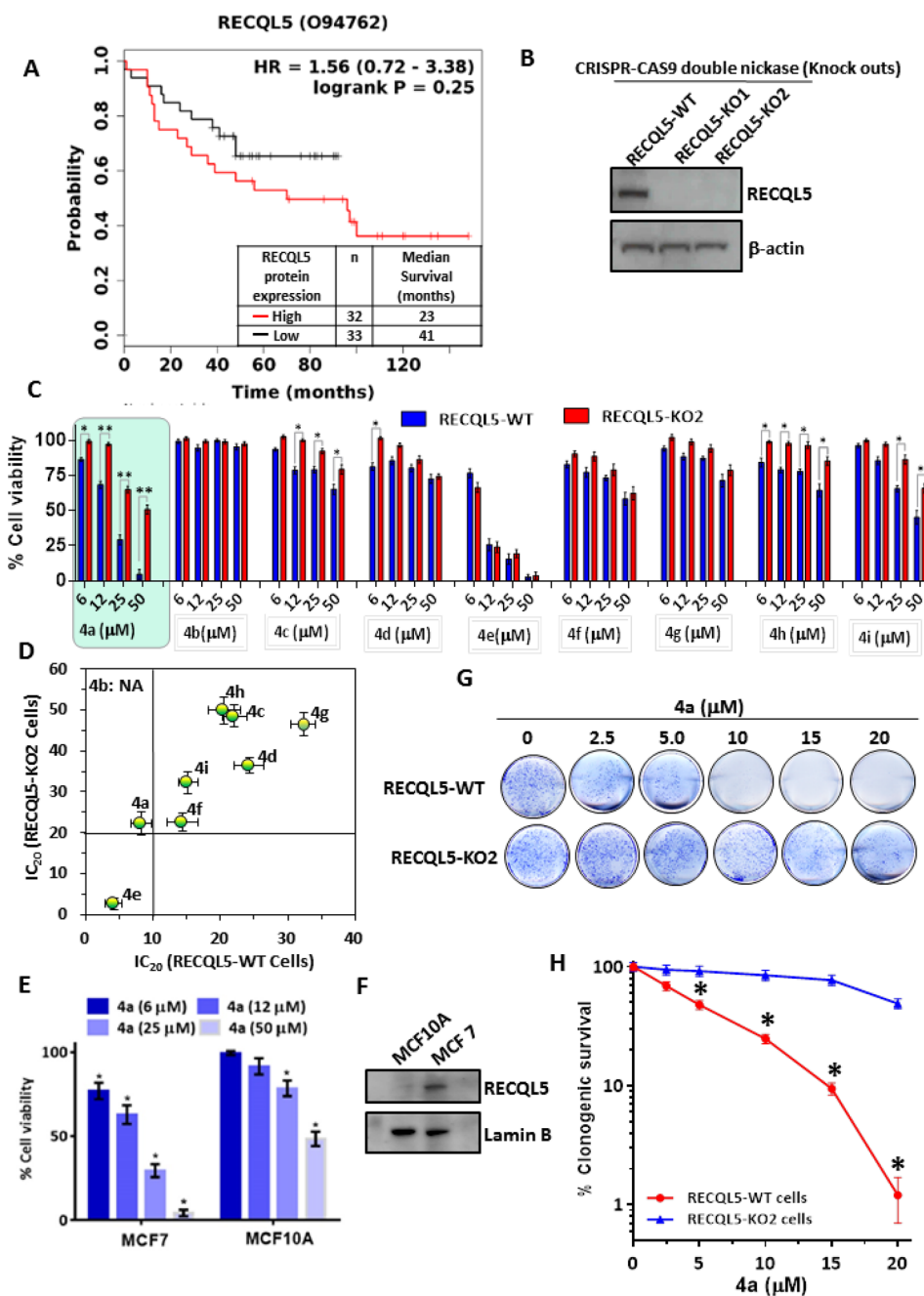


**Figure 1.** Screening and evaluation of selective cytotoxicity of 1,3,4-Oxadiazole derivatives to RECQL5-expressing breast cancer cells. (A) Kaplan–Meier analyses of overall survival of breast cancer patients with high and low RECQL5 protein expressions. (B) CRISPR-CAS9 double nickase-mediated knockout of RECQL5 in MCF-7 cells. Control double nickase plasmid and two different RECQL5 double nickase plasmids were transfected to MCF-7 cells to generate RECQL5-WT, RECQL5-KO1, and RECQL5-KO2 cells. (C) Cell viability of RECQL5-WT and RECQL5-KO2 cells after 72 h treatment with compounds 4a–i. Highlighted green box shows the highest preferential killing ability of 4a for RECQL5-WT cells. Data are shown as mean  $\pm$  SD ( $n = 4$ ). \* $p < 0.05$  and \*\* $p < 0.01$ . (D) Dot-plot of IC<sub>50</sub> values of compounds 4a–i for RECQL5-WT and RECQL5-KO2 cells. (E) Cell viability of normal mammary epithelial cells (MCF10A) vs malignant breast cancer cells (MCF-7) in response to 4a treatment (72 h). Data are shown as mean  $\pm$  SD ( $n = 4$ ). \* $p < 0.05$  w.r.t the viability of the respective vehicle-treated cells (100%). (F) RECQL5 expression in MCF10A and MCF-7 cells. (G,H) Clonogenic potential of RECQL5-WT and RECQL5-KO2 cells after 8–10 days treatment with compound 4a. Data are shown as mean  $\pm$  SD ( $n = 5$ ). \* $p < 0.01$  in comparison to respective 4a concentration in RECQL5-KO2 cells.

RECQL5 CRISPR-CAS9 plasmid systems efficiently knocked out RECQL5 in MCF-7 breast cancer cells (RECQL5-KO1 and RECQL5-KO2), in comparison to control plasmids in MCF-7 cells (RECQL5-WT) (Figure 1B). In-house library (200 drugs) comprises a small collection of chemotherapeutics, antidiabetic, antiseizure, antipsychotic, antibiotic, antiviral agents, nonsteroidal anti-inflammatory drugs, and so forth.

From our screening, we found that 1,3,4-Oxadiazole derivative molecule (e.g., Raltegravir) showed some potential to differentially kill RECQL5-WT cells over RECQL5-KO2 cells. 1,3,4-Oxadiazole derivatives are generally considered as privileged small molecules in medicinal chemistry because of their lower lipophilicity, enhanced water solubility, superior hydrolytic and metabolic stability, and improved cell

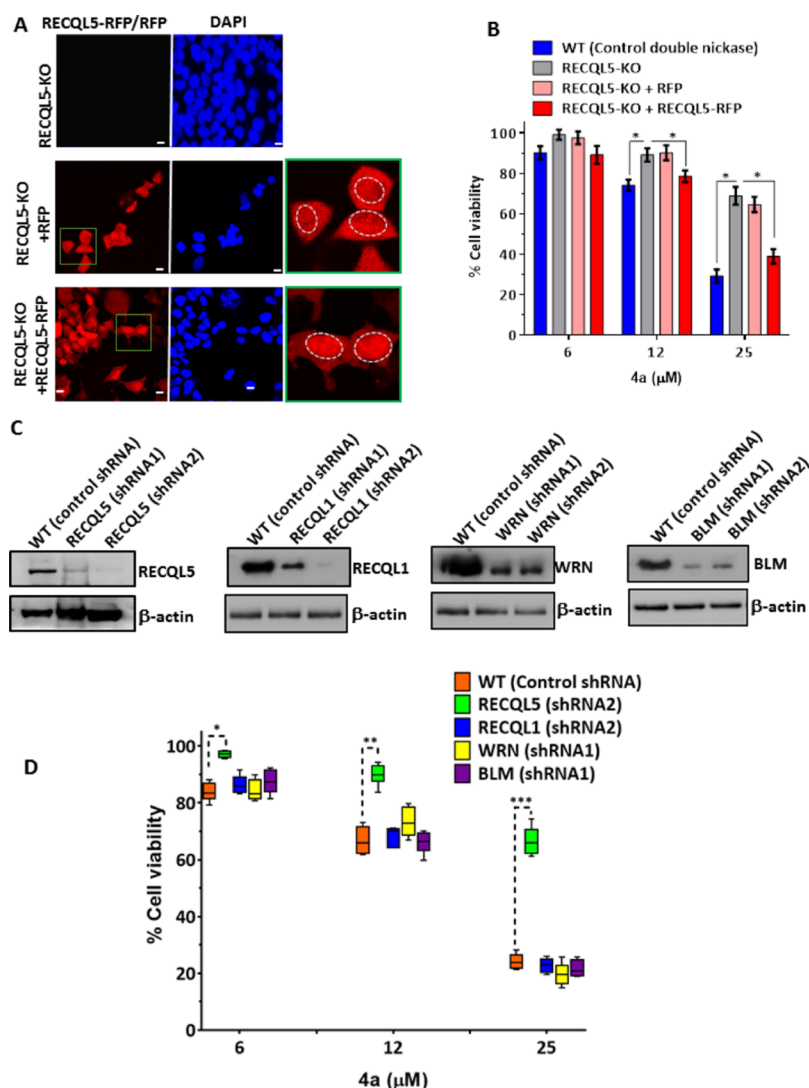


**Figure 2.** Compound 4a-mediated selective killing is dependent on the RECQL5 expression in the cancer cells. (A) Expression of RFP (control) and RECQL5-RFP in RECQL5-KO cells. Bar: 10 μm. (B) Cell viability of RECQL5-WT, RECQL5-KO, RECQL5-KO + RFP, and RECQL5-KO + RECQL5-RFP cells after 4a treatment for 72 h. Data are shown as mean ± SD ( $n = 5$ ). \* $p < 0.01$ . (C) Expression of RECQL5, RECQL1, WRN, and BLM in MCF-7 cells, after knocking down (KD) by using control shRNA and two different sets of shRNA for RECQL5, RECQL1, WRN, and BLM, respectively. (D) Clonogenic potential of control MCF-7 cells, RECQL5-KD2 (RECQL5 shRNA2), RECQL1-KD2 (RECQL1 shRNA2), WRN-KD1 (WRN shRNA1), and BLM-KD1 (BLM shRNA1) MCF-7 cells after 8–10 days treatment with compound 4a. Data are shown as mean ± SD ( $n = 5$ ). \* $p < 0.05$ , \*\* $p < 0.01$ , \*\*\* $p < 0.001$ .

membrane permeability and pharmacokinetics (PKs).<sup>18</sup> Inspired by the raltegravir structure, we synthesized three 1,3,4-Oxadiazole thiourea derivatives where phenyl group was functionalized with trifluoromethyl and nitro groups at various positions (compounds 3a–3c; Scheme 1). Among these three oxadiazole derivatives, compound 3a showed some selectivity in killing RECQL5-WT cells over RECQL5-KO2 cells (Figure S1A). In order to further enhance the selectivity, we introduced the following changes in 1,3,4-Oxadiazole derivative: (1) thiourea was replaced with urea; (2) a bulky phenyl or phenyl methyl was introduced in between urea and 1,3,4-Oxadiazole groups; and (3) phenyl group was functionalized with methoxy, methyl, trifluoromethyl, or nitro group at various positions (compounds 4a–i; Scheme 2). As shown in Figure 1C,D, all the compounds, except 4b, reduced cell viability of both RECQL5-WT and RECQL5-KO2 cells in a concentration-dependent manner. Interestingly, compound 4a (1-(3,5-bis(trifluoromethyl)phenyl)-3-((S)-(5-(benzylthio)-

1,3,4-oxadiazol-2-yl) (phenyl) methyl) urea) showed significantly higher selectivity in killing RECQL5-WT cells *vis-à-vis* RECQL5-KO cells. The IC<sub>20</sub> value (concentration at which 20% killing is achieved) of 4a was  $8.2 \pm 2.6 \mu\text{M}$  for RECQL5-WT cells, which was  $\sim 2.7$  times lower than the IC<sub>20</sub> value for RECQL5-KO2 cells ( $22.3 \pm 2.1 \mu\text{M}$ ) (Figure 1C,D). From structure activity analyses, we found that the presence of 3,5-bis(trifluoromethyl)phenyl, urea, and immobile phenyl groups in between the urea and 1,3,4-oxadiazole moiety is required for the selective killing of RECQL5-expressing cells (compounds 4a–4i; Scheme 2, Figure 1C,D). Changes in any of these chemical entities led to drastic reduction in either efficacy and/or selective killing of RECQL5-WT cells. In order to assess the cytotoxicity of 4a toward normal mammary epithelial cells (expressing RECQL5), MCF10A cells and its counter malignant MCF-7 cells were treated with 4a. Our results showed that although 4a was cytotoxic toward both the cells, IC<sub>20</sub> for MCF10A ( $33.4 \pm 3.2 \mu\text{M}$ ) was  $\sim 4$  times higher than

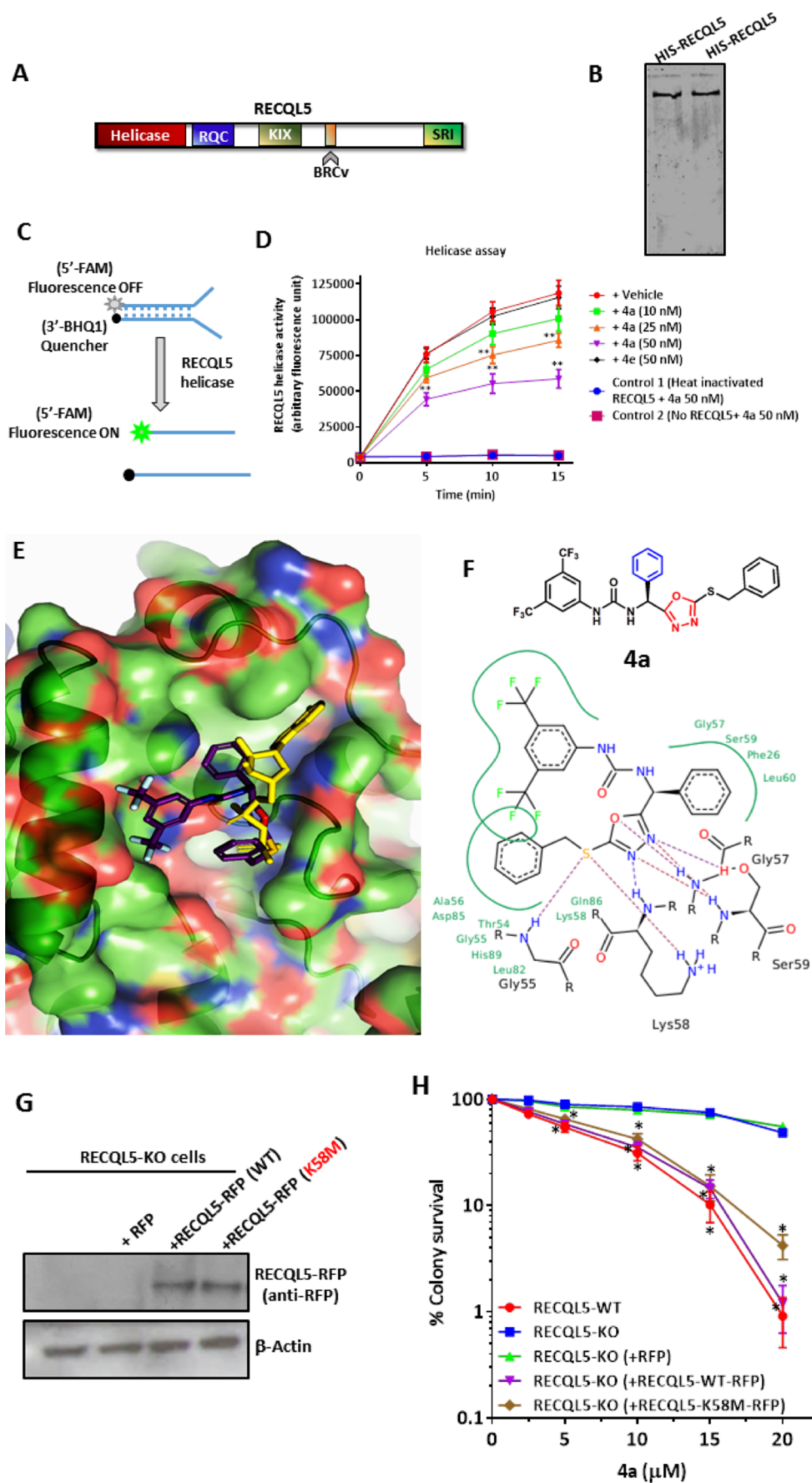
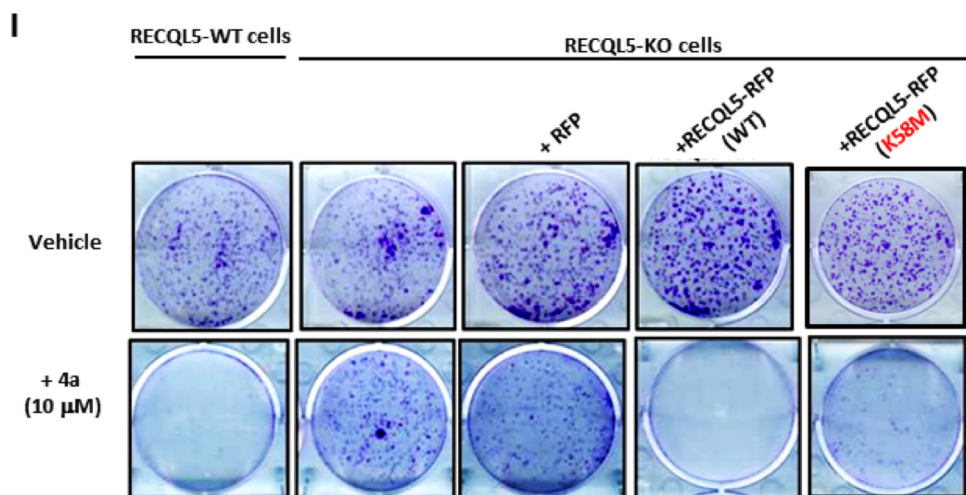


Figure 3. continued



**Figure 3.** Effect of **4a** on the ATPase, helicase, and DNA binding abilities of RECQL5 protein. (A) Schematic representation of RECQL5 protein with different domains. (B) N-terminal HIS-tagged human RECQL5 was expressed in *E. coli* and purified. The Gel shows two different batches of preparations. (C) Schematic representation of the fluorescent-based RECQL5 helicase assay using a duplex forked DNA. One of the strands was labeled with 3'-BHQ1, which quenches fluorescence of 5'-FAM labeled on the other strand. Helicase activity driven strand-unwinding results in the separation of 5'-FAM labeled strand and enhancement of the fluorescence. (D) RECQL5 helicase activity measured by the above fluorescent-based assay in the absence and presence of **4a** or **4e**. Data are shown as mean  $\pm$  SD ( $n = 5$ ).  $**p < 0.01$  and  $***p < 0.001$ . (E) Predicted binding mode of **4a** with ATPase pocket of RECQL5 (PDB code: SLB3). The diagram shows compound **4a** in purple and ADP in yellow. (F) Possible mode of interaction of **4a** with ADP binding pocket of RECQL5. (G) RECQL5-KO cells untreated or transfected with RFP and RECQL5 (WT)-RFP. RECQL5 (K58M)-RFP and expression of these proteins was assessed. (H,I) Clonogenic potential of the indicated cells after **4a** treatment (8–10 days). Data are shown as mean  $\pm$  SD ( $n = 5$ ).  $*p < 0.01$  w.r.t RECQL5-KO cells at the respective concentration of **4a**.

MCF-7 cells ( $8.4 \pm 2.9 \mu\text{M}$ ) (Figure 1E). In agreement with the previous report,<sup>12</sup> we observed very low expression of RECQL5 in normal mammary epithelial MCF10A cells than malignant MCF-7 cells. The lower RECQL5 expression in normal mammary epithelial cells (MCF10A) may attribute to lower cytotoxicity in response to **4a** treatment (Figure 1F).

In the clonogenic assay, RECQL5-WT cells were highly sensitive to **4a** treatment ( $\text{IC}_{50}$ :  $4.8 \mu\text{M}$ ), while RECQL5-KO2 cells were relatively fourfold resistant ( $\text{IC}_{50}$ :  $19.6 \mu\text{M}$ ) (Figure 1G,H). Similar results were also observed in RECQL5-KO1 cells (Figure S1B), suggesting that the differential effect of **4a** was not because of nonspecific effects of CRISPR plasmids. In order to assess the differential efficacy in other cancer cells, RECQL5 was knocked out in T47D (breast cancer cells; ER+/PR+/HER2-; and p53 mutant) by using two independent CRISPR-CAS9 systems or depleted in MDA-MB-231 (triple negative breast cancer; ER-/PR-/HER2-; and p53 mutant) and U2-OS cells (osteosarcoma cells; p53 WT) by using the lentiviral-mediated expression of two independent shRNAs (Figure S2A–F). In corroboration with MCF-7 results, we observed that RECQL5-expressing cancer cells (RECQL5-WT T47D, MDA-MB-231, and U2-OS) were highly sensitive to **4a** treatment, while the effect was drastically reduced when RECQL5 depleted in these cells (Figure S2A–F). Together, this result indicated that **4a** targets RECQL5-expressing cancer cells irrespective of their tissue origin and p53 status. In order to characterize **4a** and understand its mode of action, further experiments were carried out in RECQL5-WT and RECQL5-KO2 (henceforth named RECQL5-KO) MCF-7 cells.

**Specificity of Compound 4a in Preferential Killing of RECQL5 Helicase-Expressing Cancer Cells.** The above results showed that compound **4a** sensitizes RECQL5-expressing cells (RECQL5-WT) but not RECQL5-KO cells. In order to confirm that **4a**-induced cancer cell killing is mediated specifically through RECQL5, RECQL5-KO cells were

complemented with either the ectopic expression of RECQL5-RFP or RFP control (Figure 2A). Our cell viability assay showed that RECQL5-KO cells, in contrast to RECQL5-WT cells, were resistant to **4a** treatment. Meanwhile, complementation with RECQL5-RFP but not RFP reverted RECQL5-KO resistance phenotype in response to **4a** treatment (Figure 2B). RECQL5 shares homology with other human RECQL helicases, for example, WRN, BLM, RECQL4, and RECQL1.<sup>7</sup> In order to assess the specific interaction of **4a** with RECQL5 and not with any other RECQL helicases in cells, RECQL5, RECQL1, WRN, and BLM were systematically depleted by using two different sets of respective shRNA in MCF-7 cells. ShRNA-mediated depletion of RECQL5, RECQL1, WRN, and BLM was more than 90% in the respective knockdown cells (Figure 2C). Our cell viability assay showed that **4a** treatment reduced the viability of control cells while the effect of **4a** was significantly abrogated in RECQL5sh cells (Figure 2D). In contrast, the cytotoxic potential of **4a** was not affected in RECQL1sh, WRNsh, and BLMsh cells (Figure 2D). Together, these results confirm that the cytotoxicity potential of compound **4a** is mediated through its specific interaction with RECQL5 in the cellular context.

**Effect of Compound 4a on Enzymatic and Nonenzymatic Function of RECQL5 in Killing Cancer Cells.** The RECQL5 protein structure comprises (1) a conserved N-terminal domain, which includes RECA-like helicase domain (1–364 aa) and RQC domain (438–453 aa) and (2) C-terminal domain, which contains KIX, BRCv, and SRI domains (Figure 3A).<sup>19</sup> Biochemical analyses of RECQL5 revealed that the helicase domain has DNA-dependent ATPase and ATP-dependent 3'–5' helicase and Holliday junction branch migration activities. The crystal structure of RECQL5 showed that the RQC domain has a single  $\alpha$ -helix, which is essential for DNA binding and helicase activity of the enzyme.<sup>19</sup> In order to assess whether compound **4a**-mediated cytotoxicity might be

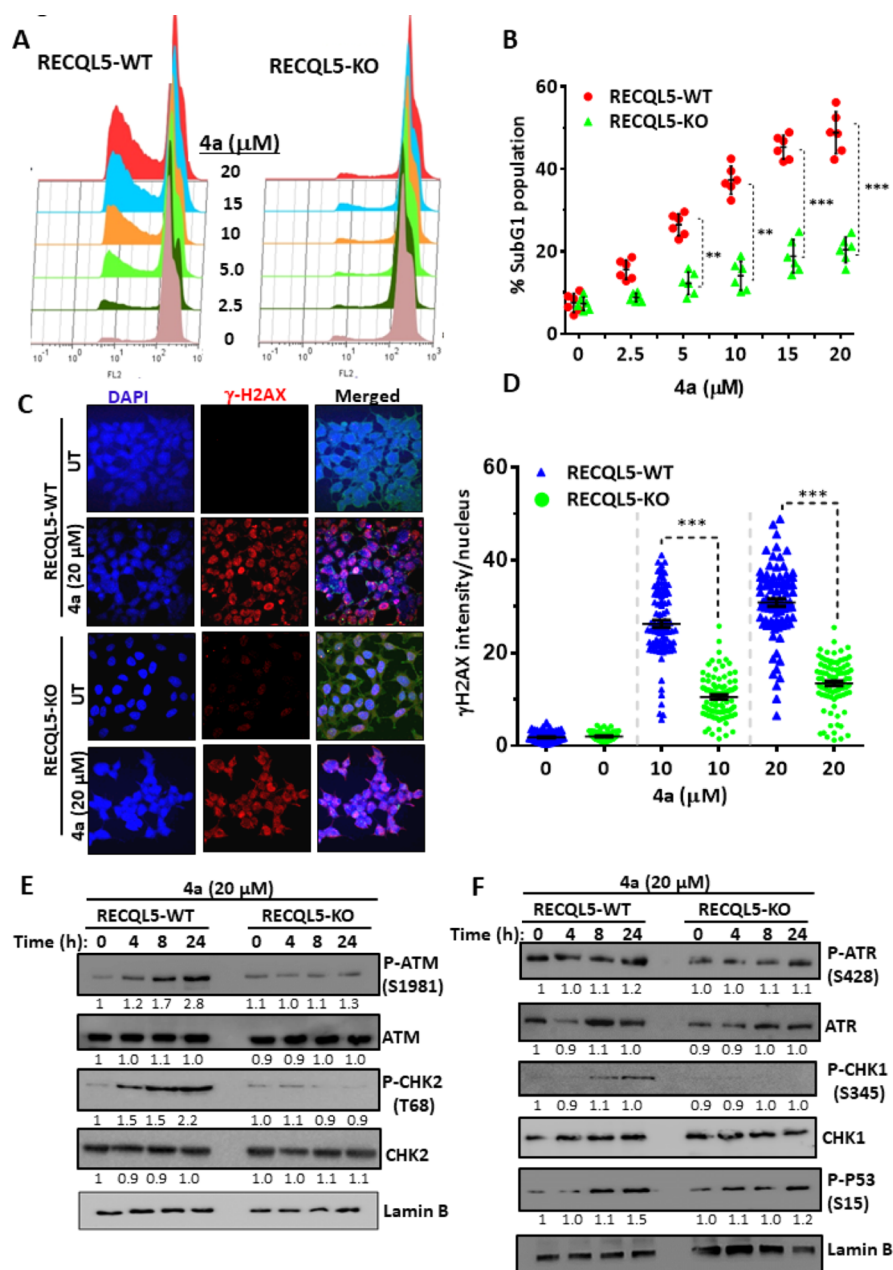


**Figure 4.** Compound **4a** caused higher accumulation of DSBs, which led to preferential death of RECQL5-expressing cells. (A,B) Apoptosis of RECQL5-WT and RECQL5-KO in response to different doses of **4a** for 72 h. Data are shown as mean  $\pm$  SD ( $n = 5$ ). \*\* $p < 0.01$  and \*\*\* $p < 0.001$ . (C,D) DSBs in the cells, treated with **4a** for 24 h, was measured by analyzing  $\gamma$ H2AX foci by immunofluorescence microscopy. Data are shown as mean  $\pm$  SEM ( $n = 5$ ). \*\*\* $p < 0.001$ . (E,F) Cells were treated with **4a** for indicated time points. DDR signaling was analyzed by western blotting. Data are shown as mean of at least three experiments.

because of its ability to inhibit ATPase, helicase, and/or DNA binding abilities of RECQL5, full length HIS-tagged human RECQL5 was expressed and purified from *E. coli* (Figure 3B). A fluorimeter-based RECQL5 helicase assay was performed by using 30-mer replication forks. One strand of this forked duplex was labeled with fluorophore (FAM) at 5'-end while the other strand was labeled with a quencher (BHQ1) at 3'-end (Figure 3C). Unwinding of this duplex due to helicase activity abolishes proximity-based fluorescence quenching of FAM by BHQ1, leading to the enhancement of FAM fluorescence that can be detected in real time. As shown in Figure S3A, wild type RECQL5 time dependently enhanced the FAM fluorescence, showing its efficient helicase activity.

The point mutation of the critical lysine residue to methionine (K577M) is known to cause loss of helicase activity of the WRN protein.<sup>20</sup> Similarly, the point mutation of the critical lysine residue to arginine (K58R)<sup>21</sup> or methionine (K58M) led to the loss of helicase activity of the RECQL5 protein (Figure S3A). Interestingly, helicase activity of the RECQL5 (WT) protein was potently inhibited in the presence of compound **4a**, in a concentration-dependent manner (IC<sub>50</sub>: 46.3 nM) (Figures 3D, S3B). Although, the compound **4e** is structurally closely related to **4a**, it showed very poor RECQL5 helicase inhibition activity in the same assay (Figure 3D). In contrast to the presence of the phenyl group in between urea and 1,3,4-Oxadiazole groups in compound **4a**, presence of the relatively

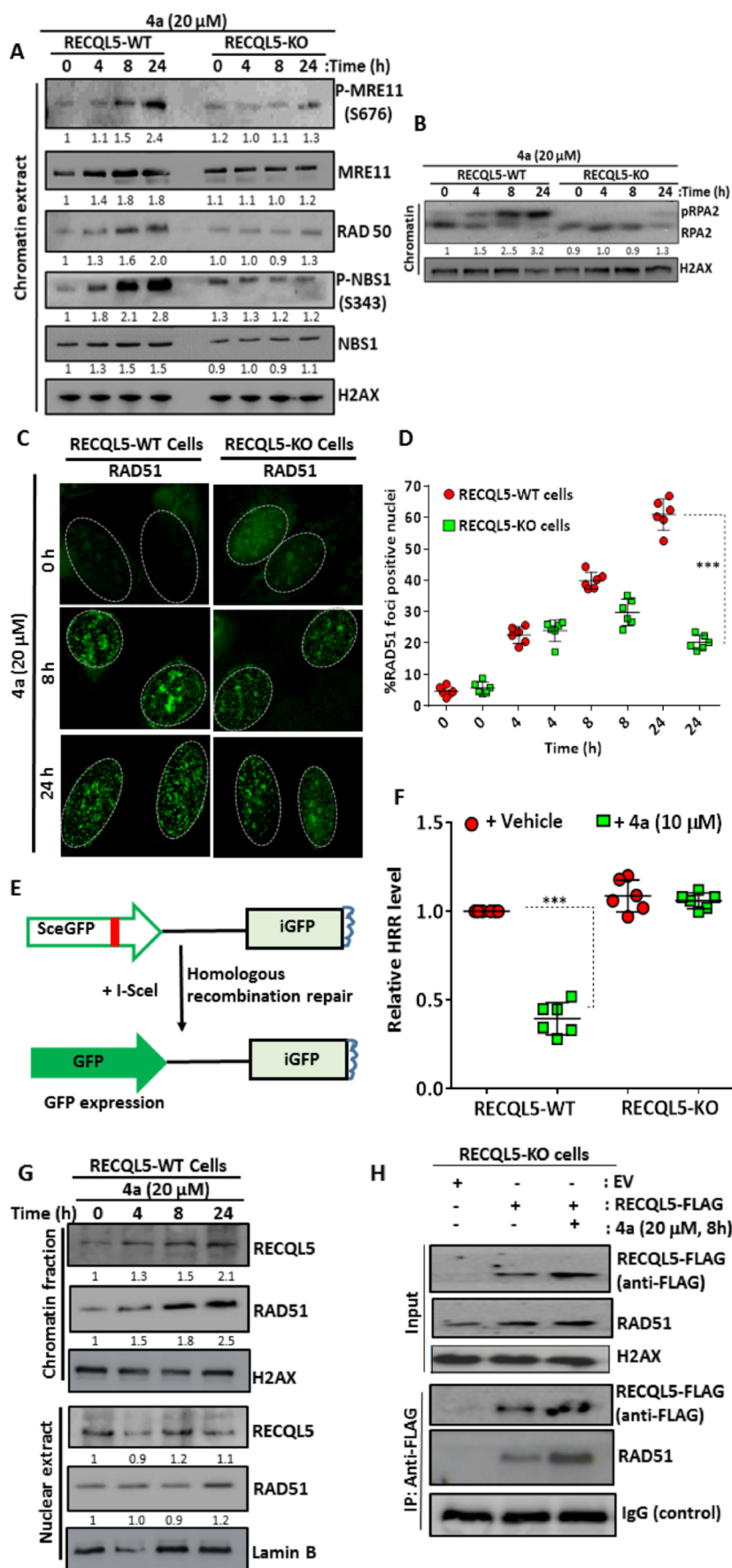
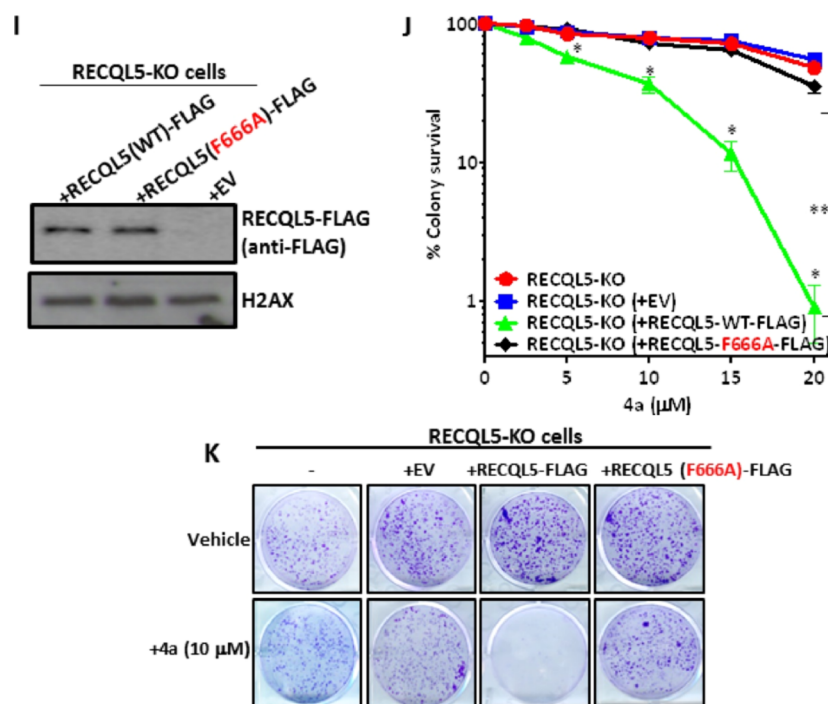


Figure 5. continued



**Figure 5.** Compound **4a**-stabilized RECQL5-RAD51 physical interaction and inhibited HRR. (A,B) RECQL5-WT and RECQL5-KO cells were treated with **4a** for indicated time points and chromatin bound proteins was analyzed by western blotting. (C,D) Cells were treated with **4a** for indicated time periods and RAD51 foci were analyzed by immunofluorescence microscopy. Highlighted box in the images were zoomed. Data are shown as mean  $\pm$  SD ( $n = 6$ ). \*\*\* $p < 0.001$ . (E) Scheme of I-SceI-induced DSBs at the SceGFP site and its HR-based repair to functional GFP. (F) Cells were treated with **4a** for 48 h and relative HRR was analyzed by measuring GFP positive cells by flow cytometry. Data are shown as mean  $\pm$  SD ( $n = 6$ ). \*\*\* $p < 0.001$ . (G) Level of RAD51 and RECQL5 in the nuclear and chromatin extract of the cells, treated with **4a**, was measured by western blotting. Data are shown as mean ( $n = 3-4$ ). (H) RECQL5-KO (MCF-7) cells transfected with EV or RECQL5-FLAG. These cells were untreated or treated with **4a**, immuno-precipitated with anti-FLAG tagged beads and probed for FLAG and RAD51. (I) RECQL5-KO (MCF-7) cells transfected with EV, RECQL5 (WT)-FLAG, and RECQL5 (F666A)-FLAG and expression of RECQL5-FLAG was assessed. (J,K) Clonogenic potential of indicated cells after **4a** treatment (8–10 days). Data are shown as mean  $\pm$  SD ( $n = 5$ ). \* $p < 0.05$  w.r.t RECQL5-KO cells at the respective concentration of **4a**. \*\* $p < 0.01$ .

more mobile phenyl methyl group in compound **4e** drastically affects its efficacy to inhibit RECQL5 (Scheme 2). In control experiments, we found that heat inactivated helicase or **4a** alone was unable to unwind duplex DNA (Figure 3D). In contrast, our *in vitro* biochemical assay showed that **4a** was not able to abrogate RECQL5 binding to the DNA substrate, even at higher concentrations (10  $\mu$ M) (Figure S3C,D). A similar result was also observed at lower concentrations of **4a**. In the ATPase assay, we found that **4a** was able to reduce DNA-dependent ATPase activity of RECQL5 in a concentration-dependent manner (Figure S3E). However, **4a** could suppress  $\sim 50\%$  of ATPase activity at higher concentrations (IC<sub>50</sub>: 23.9  $\mu$ M), suggesting a weak ATPase inhibition property of **4a** (Figure S3E). Further, we carried out molecular docking simulation of **4a** and **4e** with the ATPase domain by using the reported crystal structure of RECQL5 helicase complexed to ADP (PDB code: 5LB3) using LeadIT incorporated in BioSolveIT software. The most favorable binding mode of **4a** with ATPase pocket of RECQL5 is shown in Figure 3E,F. In this docking study, compound **4a** showed (1) hydrophobic interaction with the pockets comprising Thr54, Gly55, and Ala56 and Gly57, Ser59, Phe26, and Leu60 and (2) hydrogen bonding interactions with Gly55, Gly57, Lys58, and Ser59. In contrast to binding of **4a** (Docking score: 21), the binding of **4e** (Docking score: 6) to ATPase pocket was less favorable by  $\Delta G$ : 10 kJ/mol, because of the dynamic nature of the phenyl methyl group, leading to weaker hydrophobic and hydrogen

bonding interactions (Figure S3F,G). Together, these results suggest that **4a** is a potent inhibitor of RECQL5 helicase activity while affecting ATPase activity partially. A similar effect was reported for a WRN helicase specific inhibitor.<sup>22</sup> In order to further assess whether the potent inhibition of RECQL5 helicase (enzyme) activity might be attributable to its preferential killing of RECQL5-expressing cancer cells, a RECQL5 mutant with helicase dead function<sup>21</sup> was generated. This was carried out by introducing a point mutation (K58M) in RECQL5 through the site directed mutagenesis protocol. Our clonogenic assay result showed that RECQL5-KO cells, in contrast to RECQL5-WT cells, were resistant to **4a** treatment. Of note, the complementation of RECQL5-KO cells with either RECQL5-RFP (WT) or RECQL5-RFP (K58M) helicase dead mutant (Figure 3G) caused robust sensitization of cancer cells in response to **4a** treatment (Figure 3H,I). The effect of **4a** on RECQL5-RFP (K58M) helicase dead mutant was slightly less than RECQL5-RFP (WT) expressing cells. Together, these results suggest that the compound **4a**-mediated potent inhibition of RECQL5 helicase (enzyme) may partially confer to its preferential killing of RECQL5-expressing cancer cells. In addition to helicase enzyme activities, **4a** may possibly target the nonenzymatic function of RECQL5, leading to the robust sensitization of RECQL5-expressing cancer cells.

**Effect of Compound 4a on Double Strand Breaks Repair and DNA Damage Response.** In order to gain insights into

the molecular mechanism of preferential killing of RECQL5-expressing cancer cells, we evaluated the effects of **4a** on the double strand break (DSB) repair process. In corroboration with our cell viability and clonogenic assay results (Figure 1D,G), Compound **4a** treatment induced a significantly higher amount of apoptosis (sub-G1) in RECQL5-WT cells *vis-à-vis* RECQL5-KO cells, in a dose-dependent manner (Figure 4A,B). At 20  $\mu$ M of **4a**, ~2.5-fold higher death was observed for RECQL5-WT cells as compared to RECQL5-KO cells. Besides, **4a** treatment also induced higher death in RECQL5-WT as compared to RECQL5-depleted U2-OS and MDA-MB-231 cells, suggesting that **4a** preferentially kills RECQL5-expressing cancer cells irrespective of its cancer types (Figure S4A,B; data not shown for MDA-MB-231). Of note, 1,3,4-oxadiazole derivatives have the propensity to induce DNA damage.<sup>23,24</sup> Because RECQL5 is known to play a pivotal role in DNA damage response (DDR) and repair, it might be possible that compound **4a** inhibits RECQL5-mediated signaling and/or DNA repair, leading to a higher cell death. In the absence of RECQL5 in RECQL5-KO cells, DNA damage might be repaired through redundant compensatory proteins/pathways. In this regard, we assessed DSBs by analyzing  $\gamma$ H2AX foci in cells. As shown in Figure 4C,D, the treatment of **4a** (24 h) led to a significantly higher amount of  $\gamma$ H2AX foci in RECQL5-WT cells than RECQL5-KO cells. The  $\gamma$ H2AX foci amount was enhanced in a **4a** dose-dependent manner. Similar results were also observed in T47D cells (RECQL5-WT and RECQL5-KO cells) (Figure S4C). Further, major DDR, for example, ATM-CHK2, ATR-CHK1, and p53 signaling was remarkably elicited with higher intensities in RECQL5-WT cells *vis-à-vis* RECQL5-KO cells in response to **4a** treatment (Figure 4E,F). Taken together, our results suggested that compound **4a** induces DNA DSBs and targets the RECQL5-mediated processing of DSBs, leading to preferential killing of RECQL5-expressing cancer cells.

**Role of Compound 4a in Homologous Recombination and Stabilization of the RECQL5-RAD51 Complex.** Because compound **4a** causes robust accumulation of  $\gamma$ H2AX in RECQL5-WT cells than RECQL5-KO cells, we further systematically evaluated the effect of **4a** on NHEJ- and HR-mediated DSB repair. Initially for NHEJ and HR repair, **4a** treatment-mediated time-dependent accumulation of key NHEJ/HRR proteins on chromatin was evaluated. We found no significant difference in the rate of accumulation of KU80 and DNA-PKc on chromatin, in RECQL5-WT and RECQL5-KO cells, in response to **4a** treatment (Figure S5A). This result suggested that NHEJ might not be a crucial target of compound **4a**. Interestingly, **4a** treatment led to a time-dependent accumulation of HR processing MRN proteins, for example, MRE11, RAD50, and NBS1 on the chromatin of RECQL5-WT cells. In contrast, this effect was relatively lower in the RECQL5-KO cells. In corroboration with this result, our result revealed that the phosphorylation of MRE11 (S676) and NBS1 (S343) was significantly higher in RECQL5-WT cells *vis-à-vis* RECQL5-KO cells (Figure 5A). During HRR, DSBs are resected to generate extensive ssDNA, followed by coating and phosphorylation of RPA. In this regard, we observed ssDNA-mediated robust phosphorylation of RPA2, in a time-dependent manner, in RECQL5-WT cells in response to **4a** treatment (Figure 5B). This effect of **4a** was significantly lower in RECQL5-KO cells, suggesting that compound **4a** may target RECQL5 in a HR-mediated repair process.

Initially, it has been proposed that RECQL5 suppresses HR-mediated DSB repair by disrupting the interaction of RAD51 with ssDNA to form presynaptic filament.<sup>25,26</sup> Meanwhile, many recent studies have shown evidence that RECQL5 can also act on the postsynaptic phase during synthesis-dependent strand annealing (SDSA) process.<sup>13,15,27</sup> Hence, RECQL5 prevents the formation of aberrant RAD51 filaments on the extended invading strand and its channelization to potentially lethal cross-over pathway of HRR. Because compound **4a** has the ability to prolong MRN and ssDNA signaling in a RECQL5-dependent manner (Figure 5A,B), **4a** might be regulating RAD51 and RECQL5 physical interaction in the cells. To test this hypothesis, the kinetics of RAD51 foci formation was evaluated. Our results revealed that although the initial rate of RAD51 foci formation was similar (4 h) in both RECQL5-WT and RECQL5-KO cells (Figure 5C,D), it was enhanced at 8 h in RECQL5-WT cells. Further, a remarkably higher number of RECQL5-WT cells showed enhanced number of RAD51 foci than RECQL5-KO cells at 24 h of **4a** treatment (Figure 5C,D; Figure S5B). Similar results were also observed for T47D (RECQL5-WT and RECQL5-KO) cells (Figure S5C). The difference in the RAD51 foci level in both the cells was not because of the differential effect of **4a** on the cell cycle of the RECQL5-WT and RECQL5-KO cells (Figure S6A). This suggests that compound **4a** was not affecting the presynaptic complex formation of RAD51 at early time points but it might be stabilizing the RAD51-RECQL5 physical interaction later, leading to the suppression of further HRR. To validate **4a**-mediated HRR inhibition, we used a plasmid (pDR-GFP)-based HRR reporter assay. These cells harbor two mutant GFP genes (SceGFP and iGFP) (Figure 5E). SceGFP contains an I-SceI endonuclease site while iGFP is a truncated gene. The expression of I-SceI endonucleases leads to generation of resected DSB at the SceGFP site, which is repaired further by HR to generate functional GFP by using iGFP as a homologous template (Figure 5E). The flow cytometric measurement of GFP-expressing cells provides a measure of HRR. In this assay, we observed that HRR was significantly reduced in RECQL5-WT cells, while it was not altered in RECQL5-KO cells in response to **4a** treatment (48 h; Figure 5F). This result confirms that compound **4a** targets RECQL5 to inhibit HRR.

Because our results indicated that **4a** inhibits HRR (Figure 5D) by stabilizing the RAD51-RECQL5 physical interaction in RECQL5-expressing cells (Figure 5A,B), we carried out a series of experiments to assess the role of **4a** in stabilizing the RECQL5-RAD51 complex and its role in cancer cell death. (1) Treatment of **4a** led to the enhanced accumulation of chromatin-bound RECQL5 and RAD51, in a time-dependent manner in RECQL5-WT cells (Figure 5G). Further, RECQL5 and RAD51 levels did not alter significantly in the nuclear extracts of **4a**-treated cells (Figure 5G), indicating that **4a**-mediated accumulation of RECQL5 and RAD51 was not because of the change in the expression levels of these proteins. (2) In order to characterize the stabilization of the RECQL5-RAD51 complex by **4a**, RECQL5-KO cells were complemented with RECQL5-FLAG (WT) and treated with **4a** for 8 h and RECQL5-FLAG was pulled/immuno-precipitated (IP) by agarose beads coated with anti-FLAG. In corroboration with a previous report,<sup>14,28</sup> we found that RAD51 was co-precipitated in the RECQL5-FLAG IP sample from untreated cells (Figure 5H). Interestingly, **4a** treatment significantly enhanced the level of RAD51 in the RECQL5-FLAG IP

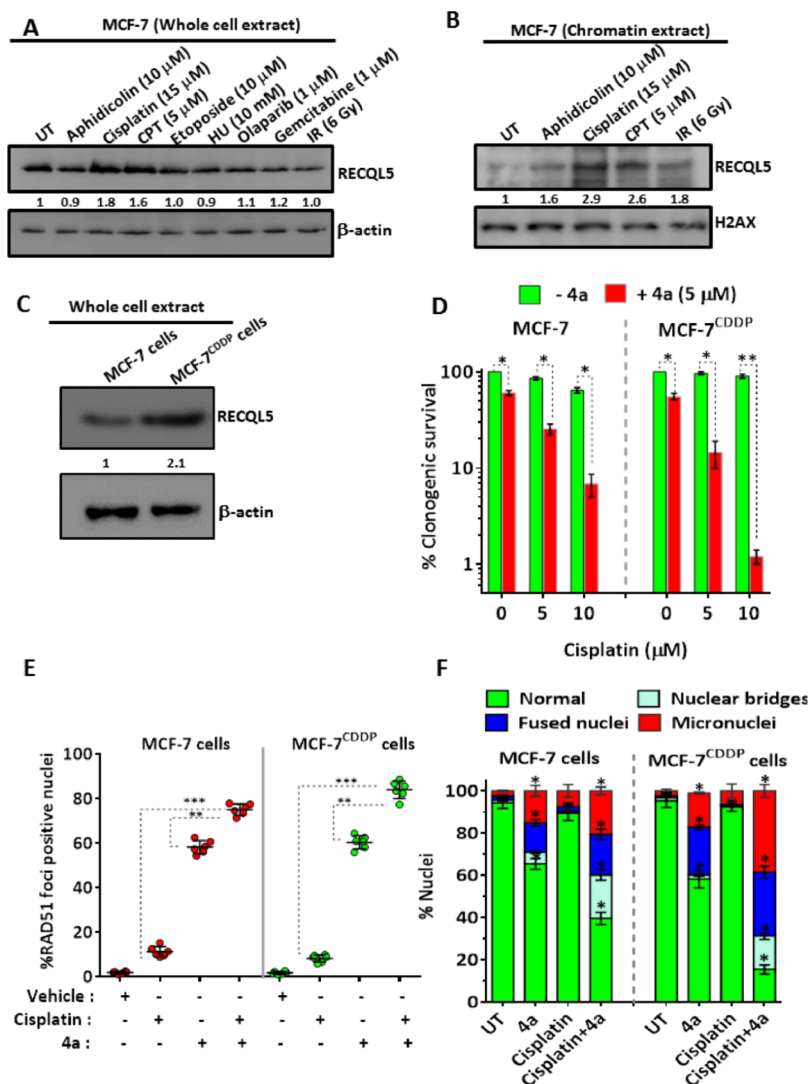


**Figure 6.** Compound 4a-abrogated *de novo* and acquired cisplatin resistance in breast cancer cells. (A) MCF-7 cells were treated with IR (6 Gy, 24 h recovery) or with indicated therapeutics for 24 h. The level of RECQL5 in whole cell extract was analyzed by western blotting. (B) MCF-7 cells were treated with IR (6 Gy, 24 h recovery) or aphidicolin, cisplatin, and CPT for 24 h. The level of chromatin-bound RECQL5 was analyzed by western blotting. (C) Cisplatin-resistant (MCF-7<sup>CDDP</sup>) cells were generated after repeated and prolonged cisplatin treatment to MCF-7 cells. Expression of RECQL5 in MCF-7 and MCF-7<sup>CDDP</sup> cells were analyzed by western blotting. (D) MCF-7 and MCF-7<sup>CDDP</sup> cells were treated with cisplatin for 8 h, cisplatin was removed and cells were treated with 4a. Clonogenic potential of these cells was assessed after 8–10 days. Data are shown as mean  $\pm$  SD ( $n = 4$ ). \* $p < 0.05$  and \*\* $p < 0.01$ . (E) MCF-7 and MCF-7<sup>CDDP</sup> cells were treated with cisplatin (20  $\mu$ M) for 8 h, cisplatin was removed and cells were treated with 4a (20  $\mu$ M) for 24 h. RAD51 foci was analyzed by immunofluorescence microscopy. Data are shown as mean  $\pm$  SD ( $n = 6$ ). \*\* $p < 0.01$  and \*\*\* $p < 0.001$ . (F) Cells were treated as mentioned in E and mitotic catastrophe was analyzed by immunofluorescence microscopy. Data are shown as mean  $\pm$  SD ( $n = 6$ ). \* $p < 0.05$  w.r.t respective untreated nuclei.

sample (Figure 5H). A similar but higher pulldown of RAD51 along with RECQL5-FLAG was observed in T47D cells (Figure S6B). Because this IP experiment was carried out with the chromatin extract, subjected with nuclease and EtBr treatment it overrules intermediacy of DNA in the RECQL5-RAD51 interaction. The IP result confirms that 4a targets RECQL5 to stabilize the RECQL5-RAD51 physical interaction to suppress HRR (Figure 5F). (3) Several recent reports showed that single amino acid mutation at the 666<sup>th</sup> position in RECQL5 abolishes its anti-recombinogenic property via abrogating its interaction with RAD51.<sup>14,28,29</sup> In this regard, we ectopically expressed RECQL5 (WT)-FLAG or RECQL5-F666A-FLAG in RECQL5-KO cells (Figure 5I) and assessed their sensitivity toward 4a treatment. In corroboration with our previous results, the colony forming ability was severely

reduced when RECQL5-KO cells were complemented with the expression of RECQL5 (WT)-FLAG protein, while transfection with empty vector (EV) had no effect (Figure 5J,K). Interestingly, RECQL5-KO cells ectopically expressing RECQL5-F666A-FLAG were almost equally resistant as RECQL5-KO cells in response to 4a treatment (Figure 5J,K). Taken together, our results confirm that 4a targets RECQL5 (WT) protein to stabilize the RECQL5-RAD51 physical interaction on chromatin (Figure 5G,H), leading to longer postsynaptic RAD51 filaments/foci (Figure 5C,D), impaired HRR (Figure 5E,F), and enhanced cytotoxicity of RECQL5-expressing cells (Figure 5J,K). In the absence of RECQL5 in KO cells, the RAD51 filament might be processed further by known RAD51 filament-disrupting factors, for example, RAD54 and BLM,<sup>13,15</sup> leading to low cytotoxicity.

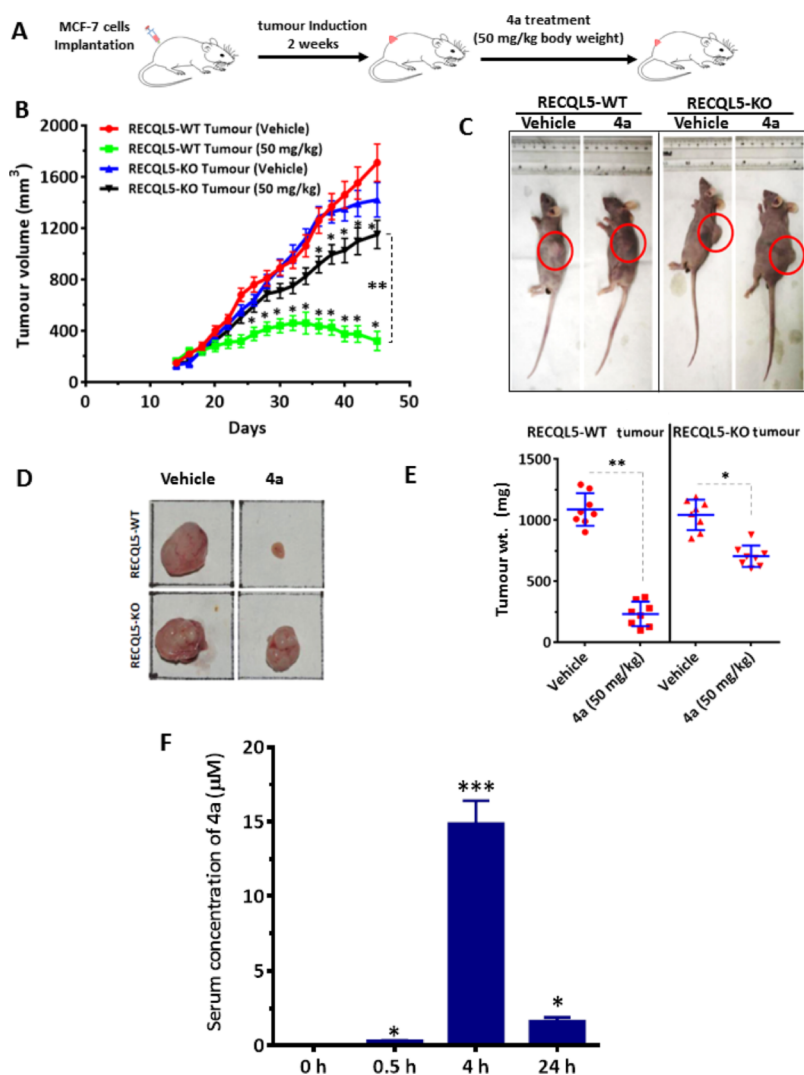


**Figure 7.** Efficacy of compound **4a** against the breast tumor in the preclinical mice model. (A) Schematic representation of the breast tumor (xenograft) development in NUDE mice and treatment protocol. (B–E) NUDE mice-bearing RECQL5-WT and RECQL5-KO tumors were treated with the vehicle or **4a** for 30 days. Tumor volume (TV) was assessed on every alternate day and plotted. Representative images of mouse bearing tumors and excised tumors are shown. Data are shown as mean  $\pm$  SD ( $n = 8$ ).  $*p < 0.05$  w.r.t respective the vehicle-treated mice.  $**p < 0.01$ . (F) Mice were given oral gavage of **4a** (50 mg/kg body wt.). Blood was collected immediately after sacrificing mice, at different time points. **4a** was extracted from the serum and subjected to HPLC analysis. The serum concentration of **4a** is shown. Data is shown as mean  $\pm$  SD ( $n = 4$ ).  $*p < 0.05$ ,  $***p < 0.01$  w.r.t 0 h.

**Effect of Compound 4a on Targeting RECQL5 in Cisplatin-Treated Breast Cancer Cells.** HRR plays a crucial role in inducing *de novo* and acquired resistance in cancer cells in response to many cancer therapeutics.<sup>29,30</sup> We hypothesized that **4a** treatment may be effective to target RECQL5 in HRR to abrogate *de novo* and acquired resistance in cancer cells in response to some of the clinically used DNA damaging cancer therapeutics. To test this hypothesis, we assessed enhancement of RECQL5 expression as a DDR to a range of clinically used DNA damaging cancer therapeutics, for example, aphidicolin, cisplatin, camptothecin (CPT), hydroxyurea (HU), olaparib (PARP inhibitor), gemcitabine, and ionizing radiation (IR). As shown in Figure 6A, an enhanced expression of RECQL5 was found in response to cisplatin and CPT. We observed that the level of chromatin-bound RECQL5 was enhanced several folds in response to aphidicolin, cisplatin, CPT, and IR treatment, suggesting a putative role of RECQL5 in *de novo* resistance to these therapeutics (Figure 6B). Previously, Hosono *et al.*

showed that RECQL5 controls HRR of DNA cross-linking and mediates cell resistance in response to cisplatin treatment.<sup>15</sup> In another study, Røe *et al.* showed that the overexpression of RECQL5 in mesothelioma cancer is associated with cisplatin resistance.<sup>16</sup>

In order to evaluate the association of RECQL5 overexpression in acquired cisplatin resistance in breast cancer cells, we generated cisplatin-resistant MCF-7 breast cancer cells by following our previously reported protocol.<sup>31</sup> The clonogenic assay showed that IC<sub>50</sub> of cisplatin was 6.9 and 18.2  $\mu$ M for parental MCF-7 and cisplatin-resistant MCF-7 (MCF-7<sup>CDDP</sup>) cells, respectively. Interestingly, we found that the expression of RECQL5 was twofold in MCF-7<sup>CDDP</sup> cells *vis-à-vis* MCF-7 cells (Figure 6C). Further, combination treatment of cisplatin and **4a** caused robust sensitization of both MCF-7 and MCF-7<sup>CDDP</sup> cells, suggesting the role of **4a** in abrogating *de novo* resistance in MCF-7 cells and acquired resistance in

MCF-7<sup>CDDP</sup> cells. The sensitizing effect of **4a** was higher in the latter cells (Figure 6D).

Then, we also noticed that the combination treatment of cisplatin and **4a** led to a higher number of RAD51 foci positive MCF-7 and MCF-7<sup>CDDP</sup> cells (Figure 6E). Again, the effect of **4a** on the stabilization of RAD51 foci was higher in MCF-7<sup>CDDP</sup> cells than MCF-7 cells. Deregulated HRR is known to induce mitotic catastrophe and cell death.<sup>32</sup> In this regard, our results showed that although individual treatment led to enhancement of mitotic catastrophe (micronuclei, nuclear bridges and fused nuclei), combination treatment of cisplatin and **4a** resulted in higher number of nuclei with mitotic catastrophe phenotype in MCF-7 and MCF-7<sup>CDDP</sup> cells (Figure 6F). Together, our results suggested that *de novo* and acquired cisplatin resistance was mediated through higher expression of RECQL5 in breast cancer cells, which is consistent with previous reports.<sup>15,16</sup> Imperatively, compound **4a** targets RECQL5 to stabilize the RECQL5-RAD51 complex, leading to the sensitization of cisplatin-resistant breast cancer cells. Hence, compound **4a** may act as an excellent adjuvant for cisplatin therapy of breast cancer.

**Pharmacodynamic (PD) Effects of Compound 4a on Reduction of Breast Tumor in Preclinical NUDE Mouse Model.** The above results demonstrated the ability of compound **4a** to target RECQL5 and preferentially kill RECQL5-expressing cancer cells *in vitro*. To assess the PD effects of **4a** on RECQL5 target in tumor, we used NUDE mice-bearing RECQL5-WT and RECQL5-KO breast xenograft tumors. In this regard, our result showed that oral gavage of compound **4a** (50 mg/kg body weight; alternate day; 30 days) (Figure 7A) robustly reduced the growth of RECQL5-expressing tumor in a time-dependent manner (Figure 7B–E). In contrast, the effect of compound **4a** was significantly lower against RECQL5-KO breast cancer in NUDE mice (Figure 7B–E). Further, the oral gavage of compound **4a** was well tolerated without any sign of weight loss (Figure S7A) or morphological abnormality in major organs, for example, liver, kidney, spleen, lungs, and heart. Pharmacodynamically, these results showed that the oral administration of compound **4a** was also effective in targeting RECQL5-expressing breast tumors *in vivo* preclinical models.

**PKs and Toxicity Effect of 4a in Preclinical Mouse Models.** In order to assess the PK of **4a**, mice were given the oral gavage of **4a** (one dose of 50 mg/kg body weight), and serum concentration of **4a** at different time points (0, 0.5, 4, and 24 h) was analyzed by high-performance liquid chromatography (HPLC). As shown in Figures 7E and S7B, we found that the serum concentration of **4a** was enhanced time dependently up to 4 h (~14.8  $\mu$ M), which was reduced at 24 h. This result shows that the therapeutically effective serum concentration of **4a** is achievable by oral administration. Besides, higher drug uptake by tumors may further enhance the concentration of **4a** and its antitumor efficacy. Moreover, the reduction of the serum concentration of **4a**, after 24 h of oral gavage, also suggests an efficient clearance of **4a**. For chronic toxicity, the mice were given a higher dose of **4a** (100 mg/kg body weight; oral gavage) and related changes in body weight, behavior, stool texture, food, and water uptake was monitored for one month. We observed that weight, behavior, food/water uptake, and stool texture were not changed in **4a**-treated animals *versus* vehicle-treated animals. Besides, the plasma biochemistry profile revealed no hepatic and renal toxicity in **4a**-treated *vis-à-vis* vehicle-treated mice (Table 1). To assess the effect of

**Table 1. Chronic Toxicity of 4a in the Preclinical Mouse Model<sup>a</sup>**

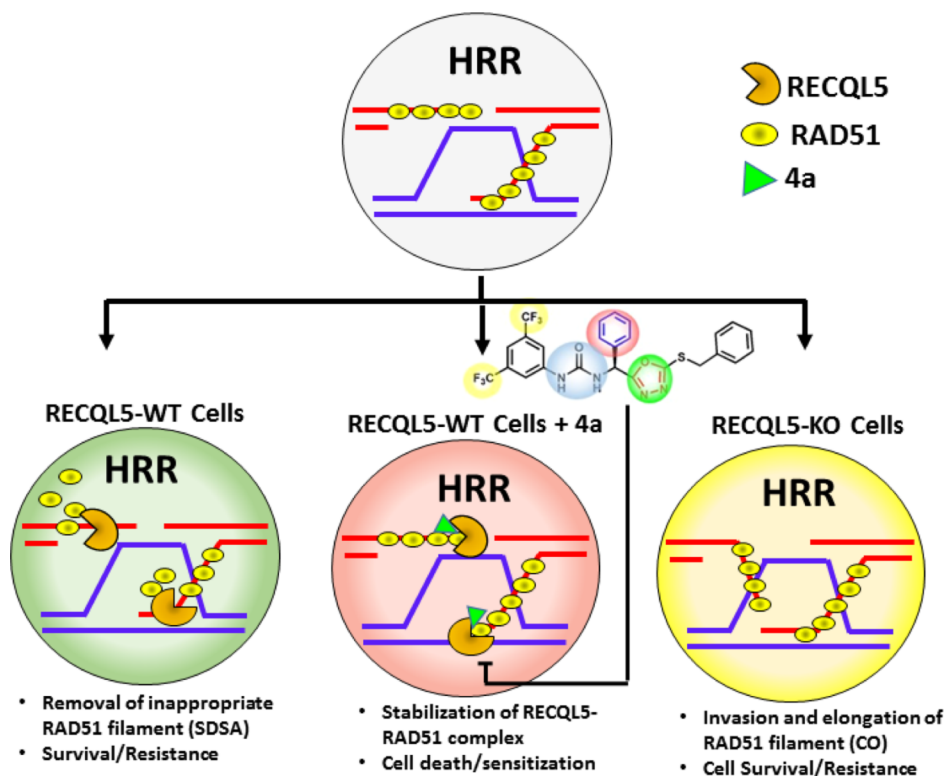
	plasma/tissue profile	<b>4a</b> -treated mice (100 mg/kg body wt) fold changes w.r.t vehicle-treated mice
1	creatinine	1.05 $\pm$ 0.1
2	SGPT	0.92 $\pm$ 0.05
3	ALP	0.97 $\pm$ 0.08
4	spleen cell count	1.03 $\pm$ 0.06

<sup>a</sup>Data are shown as mean  $\pm$  SD ( $n = 8$ ).

**4a** on the proliferating normal cells, total spleen cells were measured. As shown in Table 1, we found no appreciable changes in the cell counts in the spleen of vehicle- and **4a**-treated mice.

## DISCUSSION

Recently, several *in vitro*, preclinical and clinical studies demonstrated that cancers develop *de novo* and acquired resistance to many DNA damaging therapeutics because of the upregulation of HRR.<sup>33</sup> Thus, HRR has been an attractive target to develop small-molecule inhibitors for enhancing sensitivity of cancer cells and overcoming their resistance to chemo- and radiotherapy.<sup>30,33</sup> In this regard, small-molecule inhibitors, for example, CYT-0851 and cediranib, which inhibit HRR, currently reached different phases of clinical trials (I–III) for the treatment of cancer patients.<sup>34,35</sup> In clinical oncology, current research is mainly focused on the discovery of different druggable targets in HRR for the sensitization and treatment of different types of cancer. Recently, Bagnoloni *et al.*, discovered dihydroquinolone pyrazoline-based molecule, which inhibits HRR by disrupting RAD51-BRCA2 physical interactions and sensitizes cancers to PARP inhibitor.<sup>36</sup> Different RECQL helicases, which play important roles in the HRR process, are also considered as attractive targets for cancer therapy. In this regard, small-molecule inhibitors were developed to specifically target WRN and BLM RECQL helicases and its potential utility as an anticancer agent was advocated.<sup>22,37</sup> Interestingly, Yin *et al.* identified a class of isaindigotone derivatives, which inhibits the recruitment of BLM at the DSB sites and promotes the accumulation of unresolved RAD51 filaments/foci, leading to the death of the cancer cells.<sup>38</sup> In the current study, we discovered 1,3,4-oxadiazole derivative (compound **4a**) as a potent RECQL5 inhibitor (targeting both enzymatic and nonenzymatic domain) through synthesis, screening, biochemical assays, and *in vitro* and *in vivo* evaluation. We demonstrated that compound **4a** abrogates HRR in RECQL5-expressing cancers, leading to their robust sensitization. Because our and others' analyses have shown that the overexpression of RECQL5 is associated with serious clinicopathological conditions and poor survival in a set of breast cancer patients (Figure 1A), the inhibition of RECQL5-regulated HRR in RECQL5-expressing tumors may be therapeutically beneficial against RECQL5-expressing cancers. Among the series of synthesized 1,3,4-oxadiazole derivatives with structural diversities, compound **4a** emerged as a preferential and potent cytotoxic agent against RECQL5-expressing breast cancer, while its cytotoxic effect was drastically reduced in the absence of RECQL5 in RECQL5-KO breast cancer cells. Our results showed that compound **4a** had the ability to induce DSBs and inhibit HRR in RECQL5-expressing breast cancer cells. The preferential

Scheme 3. Schematic Representation of Mode of Action of 4a in Preferential Killing of RECQL5-Expressing Cells<sup>a</sup>

<sup>a</sup>CO: cross-over; SDSA: synthesis-dependent strand annealing.

killing of RECQL5 positive cells was associated with the ability of 4a to stabilize the RECQL5-RAD51 physical interaction at the HR sites. In the context of HRR, several findings showed that RECQL5 disrupts RAD51 filament formation by (1) abrogating the interaction of RAD51 with ssDNA, prior to D-loop formation,<sup>14,26</sup> and/or (2) removing RAD51 on the two preformed RAD51 filaments.<sup>15,27</sup> During the latter process, RECQL5 removes RAD51 on the extended invading strand and its twin noninvading strands to support SDSA and prevent a potentially hazardous cross-over during HRR (Scheme 3). Our results suggested that RAD51 foci were efficiently formed initially in both RECQL5-WT and RECQL5-KO cells in response to 4a treatment. At a latter time point, a robust accumulation of RAD51 foci was observed in RECQL5-WT cells only, suggesting that RECQL5-mediated removal of RAD51 was inhibited by stabilizing the RECQL5-RAD51 physical interaction by compound 4a (Scheme 3). Nevertheless, 4a targeted the nonenzymatic domain of RECQL5 and enhanced RAD51 foci (Figure 5C,D), RAD51 level on chromatin (Figure 5G), stabilized RECQL5-RAD51 physical interaction (Figure 5H), and suppressed HRR (Figure 5E) in RECQL5 positive cancer cells.

The ATPase and helicase activity of RECQL5 is known to influence the HRR process-mediated suppression of the sister chromatid exchange in chicken DT40 cells.<sup>28,39</sup> Interestingly, it is reported that (1) different RECQL5 mutants (including F666A), defective for RAD51 binding, have an intact helicase function and (2) RECQL5 helicase mutation (K58R) has no significant impact on RECQL5 binding to RAD51.<sup>26</sup> In this regard, breast cancer cells expressing helicase dead RECQL5 mutant (K58M) were also significantly sensitive to 4a. This suggests that although 4a potentially inhibit RECQL5 helicase

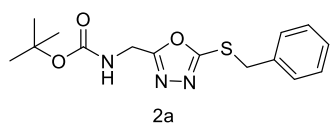
activity, this may only partially contribute to 4a-mediated killing of RECQL5-expressing cancers. In contrast, RECQL5-KO cells ectopically expressing the RECQL5 (F666A) mutant, which poorly interacts with RAD51,<sup>14,26,27</sup> were almost equally resistant as RECQL5-KO cells to 4a treatment (Figure 5K). Because the crystal structure of the C-terminal region of RECQL5 is unavailable, we were unable to assess the molecular interaction of 4a with the RAD51-interacting (BRCv) domain of RECQL5 (Figure 3A). Nevertheless, our extensive investigation in cellular studies suggested that compound 4a targets RECQL5 and stabilizes RECQL5-RAD51 physical interaction, inhibits RAD51 removal by RECQL5, leading to the accumulation of unresolved toxic RAD51 foci/filaments in RECQL5-expressing cells (Scheme 3). Because the RECQL5 expression is not only upregulated in breast cancer patients, it may also be upregulated in response to DNA damage therapeutics, leading to enhanced HRR-mediated *de novo* or acquired resistance and therapeutic failure. In this regard, our results showed remarkable enhancement in the accumulation of RECQL5 on the chromatin of breast cancer cells in response to clinically approved cancer therapeutics, for example, cisplatin, CPT, aphidicolin, and IR (Figure 6B). Recently, it has also been reported that the RECQL5 expression is associated with cisplatin resistance in different cancers.<sup>15,16</sup> In the current study, we also observed an enhanced upregulation of the RECQL5 expression in cisplatin-resistant breast cancer (MCF-7<sup>CDDP</sup>) cells than its parental MCF-7 breast cancer cells (Figure 6C). Intriguingly, combination treatment of 4a significantly enhanced RAD51 foci and robustly sensitized both MCF-7 parental and MCF-7<sup>CDDP</sup> cells to cisplatin treatment. The effect was higher in the MCF-7<sup>CDDP</sup> cells.

In conclusion, small molecule **4a** was synthetically designed to target both enzymatic and nonenzymatic domain of RECQL5 in breast cancer. Mechanistically, it stabilized RECQL5-RAD51 physical interaction, leading to the accumulation of the RAD51 filament, HRR impairment, and cell death. Together, compound **4a** may be used as a single agent to sensitize RECQL5-expressing breast cancer. It can also be used as an adjuvant with cisplatin to abort RECQL5-mediated HRR, thereby it may reduce *de novo* and acquired cisplatin resistance in breast cancer. In the preclinical mouse model, compound **4a** was orally effective in significantly reducing growth of RECQL5-expressing breast tumors as compared to RECQL5-KO tumors (Figure 7). High potency along with its nontoxic nature toward normal mammary epithelial cells (MCF10A) and different vital organs (liver, kidney, and spleen) and easy synthetic route in an appreciable quantity make **4a** a promising and attractive neo-adjuvant/adjuvant against RECQL5-expressing breast tumors.

## EXPERIMENTAL SECTION

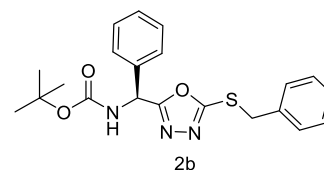
**Chemical Synthesis. Reagents, Materials, and Instrumentation.** All reagents and solvents were of the highest reagent and analytical grades and used without further purifications, unless otherwise stated. Thin-layer chromatographic plates (0.25 mm thickness, Merck Silica Gel 60F<sub>254</sub>) and MN silica gel 60 (230–400 mesh) were used for visualization and purification. The IR (KBr), <sup>1</sup>H, and <sup>13</sup>C NMR spectra were recorded with a BRUKER Tensor II Spectrophotometer Bruker AC-200 (200 MHz) or a Varian 500 MHz NMR spectrometer, respectively. Either MestReNova Lite-11.0.4, ACD/1D NMR Processor, or Bruker TOPSPIN software was used to process NMR spectra. High-resolution mass spectra (MS) were recorded on Agilent instrument and spectral analyses was carried out by 6200 series software (TOF/6500, Version Q-TOF B.05.01 B5125). All NMR spectra are shown in Figure S8. The purity of both the lead compounds (**4a** and **4e**) are >98% pure, as assessed by HPLC (JASCO; C18 column) (Figure S9).

**General Procedure for the Synthesis of 2a–2c (Schemes 1 and 2).** A mixture of a *N*-Boc-protected amino acid methyl ester (10 mmol) and hydrazine hydrate (2 mL) in absolute ethanol (10 mL) was heated under reflux for 2 h. The reaction mixture was cooled to room temperature and evaporated under reduced pressure to give the *N*-Boc amino acid hydrazide as a white solid. *N*-Boc amino acid hydrazide (10 mmol, 2.7 g) was added to a stirred solution of KOH (0.8 g, 20 mmol) in ethanol (50 mL) followed by the dropwise addition of carbon disulfide (6 mL) with vigorous stirring. The reaction mixture was heated under reflux for 4 h, brought to room temperature, and evaporated under reduced pressure. The residue was taken in water (20 mL), neutralized with 0.5 M HCl to pH 6, and extracted with ethyl acetate (3 × 10 mL). The extract was dried over anhydrous MgSO<sub>4</sub> and evaporated under reduced pressure to give crude **2a–c**. This crude product (**2a**) in dry ethanol (15 mL) was cooled in an ice-water bath and Et<sub>3</sub>N (1.1 equiv, 1.1 mL) was added followed by the addition of benzyl bromide (1.1 equiv, 1.3 mL). The reaction mixture was stirred at room temperature for 30 min and concentrated under reduced pressure. The residue was dissolved in ethyl acetate and washed with water. The organic layer was evaporated under reduced pressure and the residue was purified by column chromatography to afford pure **2(a–c)**.

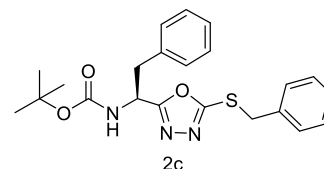


**tert-Butyl (5-(Benzylthio)-1,3,4-oxadiazol-2-yl)methylcarbamate (2a).** <sup>1</sup>H NMR (500 MHz, CDCl<sub>3</sub>): 7.39 (d, *J* = 7.0 Hz, 2 H), 7.32–7.25 (m, 3 H), 5.33 (br s, 1 H), 4.48 (d, *J* = 4.5 Hz, 1 H), 4.42 (s, 2

H), 1.43 (s, 9 H); <sup>13</sup>C NMR (125 MHz, CDCl<sub>3</sub>): 164.9, 164.6, 155.4, 135.4, 129.1, 128.8, 128.1, 80.5, 36.7, 35.8, 28.3.

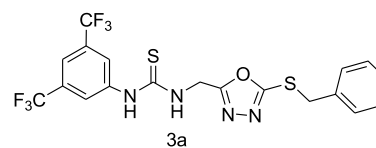


**tert-Butyl (S)-(5-(Benzylthio)-1,3,4-oxadiazol-2-yl)(phenyl)methylcarbamate (2b).** <sup>1</sup>H NMR (500 MHz, CDCl<sub>3</sub>): 7.40–7.35 (m, 5 H), 7.33–7.28 (m, 5 H), 6.08 (d, *J* = 7.0 Hz, 1 H), 5.61 (br s, 1 H), 4.42 (ABq, *J* = 13 Hz, 16.0 Hz, 2 H), 1.45 (s, 9 H); <sup>13</sup>C NMR (125 MHz, CDCl<sub>3</sub>): 166.7, 164.7, 154.5, 136.7, 135.4, 129.1, 129.0, 128.8, 128.8, 128.0, 127.1, 80.8, 51.5, 36.9, 28.3.

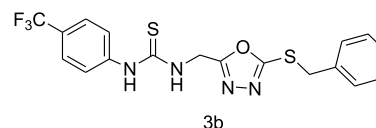


**tert-Butyl (S)-1-(5-(Benzylthio)-1,3,4-oxadiazol-2-yl)-2-phenylethylcarbamate (2c).** <sup>1</sup>H NMR (500 MHz, CDCl<sub>3</sub>): 7.40 (d, *J* = 7.0 Hz, 2 H), 7.35–7.28 (m, 4 H), 7.25–7.23 (m, 2 H), 7.08–7.07 (m, 2 H), 5.25 (d, *J* = 6.5 Hz, 1 H), 5.02 (d, *J* = 8.0 Hz, 1 H), 4.41 (s, 2H), 3.23 (dd, *J* = 6.0 Hz, 13.5 Hz, 1H), 3.15 (dd, *J* = 5.5 Hz, 12.5 Hz, 1H), 1.40 (s, 9 H); <sup>13</sup>C NMR (125 MHz, CDCl<sub>3</sub>): 167.1, 164.2, 154.7, 135.4, 135.3, 129.2, 128.9, 128.7, 128.6, 128.0, 127.1, 80.4, 48.3, 39.6, 36.8, 28.1.

**General Procedure for Synthesis of 3(a–c) (Schemes 1 and 2).** Trifluoroacetic acid (0.5 mL) was dropwise added to a stirred solution of **2a** (0.5 mmol) in dry dichloromethane (2 mL). After 2 h, solvents were removed under reduced pressure to afford the trifluoroacetate salt. A solution of crude trifluoroacetate salt (0.5 mmol) in dichloromethane (5 mL) was cooled at 0 °C in an ice-water bath. Et<sub>3</sub>N (0.1 mL, 0.55 mmol) was added followed by respective isothiocyanates (0.5 mmol) and stirred for 15 min at room temperature, the mixture was concentrated under reduced pressure and the residue was taken in ethyl acetate. The solution was washed with water and concentrated under reduced pressure. The crude product was purified by column chromatography to afford pure **3a–c**.

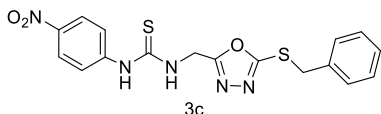


**1-(3,5-bis(trifluoromethyl)phenyl)-3-((5-(benzylthio)-1,3,4-oxadiazol-2-yl)methyl)thiourea (3a).** White solid; yield = 160 mg (65%); mp 190.2–191.0 °C; IR (neat)  $\nu_{\max}$ , cm<sup>-1</sup>: 1690 (C=S), 1655 (C=N), 3196; <sup>1</sup>H NMR (500 MHz, CDCl<sub>3</sub>): 8.17–8.12 (m, 3 H), 7.26–7.19 (m, 5 H), 4.47 (s, 2H), 3.93 (s, 2 H); <sup>13</sup>C NMR (125 MHz, CDCl<sub>3</sub>): 181.1, 170.4, 149.1, 139.2, 136.8, 130.6 (q, *J* = 31.7 Hz), 130.1, 129.0, 128.7, 127.2, 123.4 (q, *J* = 271.6 Hz), 121.9, 46.5, 32.5; HRMS (ESI): calcd for C<sub>19</sub>H<sub>14</sub>F<sub>6</sub>N<sub>4</sub>OS<sub>2</sub> (M + H)<sup>+</sup>, 493.0585; found, 493.0580.



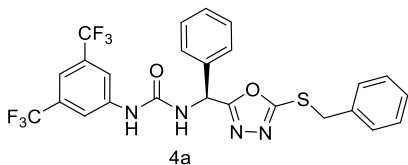
**1-((5-(Benzylthio)-1,3,4-oxadiazol-2-yl)methyl)-3-(4-(trifluoromethyl)phenyl)thiourea (3b).** White solid; Yield = (148 mg, 70%); mp 219.1–220.2 °C; IR (neat)  $\nu_{\max}$ , cm<sup>-1</sup>: 1628 (C=N), 1689 (C=S), 3154; <sup>1</sup>H NMR (500 MHz, CDCl<sub>3</sub>): 7.83 (d, *J* = 7.5 Hz, 2 H), 7.60 (d, *J* = 7.5 Hz, 2 H), 7.25–7.19 (m, 5 H), 4.51 (s, 2 H), 3.95

(s, 2 H);  $^{13}\text{C}$  NMR (125 MHz,  $\text{CDCl}_3$ ): 181.4, 169.8, 150.1, 139.2, 138.4, 129.9, 128.7, 128.4, 128.2, 126.8, 125.6, 124.1 (q,  $J = 270.8$  Hz), 46.2, 31.9; HRMS (ESI): calcd for  $\text{C}_{18}\text{H}_{15}\text{F}_3\text{N}_4\text{O}_2\text{S}$  ( $\text{M} + \text{H}$ ) $^+$ , 425.0712; found, 425.0713.

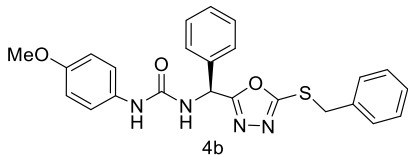


**1-((S)-5-(Benzylthio)-1,3,4-oxadiazol-2-yl)methyl)-3-(4-nitrophenyl)thiourea (3c).** White solid; yield = 136 mg (68%); mp 193.8–194.2 °C; IR (neat)  $\nu_{\text{max}}$   $\text{cm}^{-1}$ : 1688 (C=S), 1635 (C=N), 3154;  $^1\text{H}$  NMR (500 MHz,  $\text{CDCl}_3$ ): 8.30 (d,  $J = 8.5$  Hz, 2 H), 7.67 (d,  $J = 8.5$  Hz, 2 H), 4.50 (s, 2 H), 3.93 (s, 2 H);  $^{13}\text{C}$  NMR (125 MHz,  $\text{CDCl}_3$ ): 181.4, 170.1, 149.9, 146.8, 140.9, 139.5, 130.7, 129.1, 128.8, 127.2, 124.1, 46.6, 32.3; HRMS (ESI): calcd for  $\text{C}_{17}\text{H}_{15}\text{N}_5\text{O}_3\text{S}_2$  ( $\text{M} + \text{H}$ ) $^+$ , 402.0689; found, 402.0680.

**General Procedure for Synthesis of Compounds 4a–4i (Schemes 1 and 2).** Trifluoroacetic acid (0.5 mL) was dropwise added to a stirred solution of **2a–c** (0.5 mmol) in dry dichloromethane (2 mL). After 2 h, the volatiles were removed under reduced pressure to afford the trifluoroacetate salt. A solution of the crude trifluoroacetate salt (0.5 mmol) in dichloromethane (5 mL) was cooled in an ice-water bath. To it was added  $\text{Et}_3\text{N}$  (0.1 mL, 0.55 mmol), followed by the addition of respective isocyanates (0.5 mmol). After 15 min of stirring at room temperature, the mixture was concentrated under reduced pressure and the residue was taken in ethyl acetate. The solution was washed with water and concentrated under reduced pressure. The crude product was purified by column chromatography to afford compounds **4a–i**.

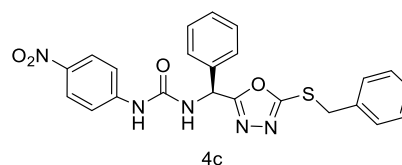


**1-(3,5-Bis(trifluoromethyl)phenyl)-3-((S)-5-(benzylthio)-1,3,4-oxadiazol-2-yl)(phenyl)methyl)urea (4a).** Yield: 207 mg (75%), white solid; mp 128–129 °C;  $[\alpha]_{\text{D}}^{25} = -2.5$  (c 1.06,  $\text{CHCl}_3$ ); IR (neat)  $\nu_{\text{max}}$   $\text{cm}^{-1}$ : 1622 (C=N), 1694 (C=O), 3360;  $^1\text{H}$  NMR (500 MHz,  $\text{CDCl}_3$ ): 8.85 (s, 1 H), 7.95–7.88 (m, 2 H), 7.58, (d,  $J = 7.5$  Hz, 1 H), 7.45 (s, 1 H), 7.36–7.27 (m, 5 H), 7.26–7.24 (m, 5 H), 6.55 (d,  $J = 7.5$  Hz, 1H), 4.38 (br s, 2 H);  $^{13}\text{C}$  NMR (125 MHz,  $\text{CDCl}_3$ ): 168.6, 165.5, 153.9, 140.9, 136.6, 134.5, 132.3 (q,  $J = 33.0$  Hz), 129.4, 129.1, 128.9, 128.8, 128.4, 126.8, 123.3 (q,  $J = 270.8$  Hz), 118.3, 115.6, 50.3, 37.3; HRMS (ESI): calcd for  $\text{C}_{25}\text{H}_{18}\text{F}_6\text{N}_4\text{O}_2\text{S}$  ( $\text{M} + \text{H}$ ) $^+$ , 553.1127; found, 553.1124.

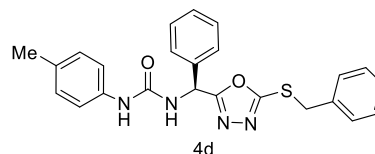


**1-((S)-5-(Benzylthio)-1,3,4-oxadiazol-2-yl)(phenyl)methyl)-3-(4-methoxyphenyl)urea (4b).** White solid; yield = 123 mg (55%); mp 158.3–159.1 °C;  $[\alpha]_{\text{D}}^{25.2} = +17.6$  (c 1.05,  $\text{CHCl}_3$ ); IR (neat)  $\nu_{\text{max}}$   $\text{cm}^{-1}$ : 1596 (C=N), 1666 (C=O), 3347;  $^1\text{H}$  NMR (500 MHz,  $\text{CDCl}_3$ ): 7.76 (s, 1 H), 7.29 (br s, 5 H), 7.25–7.24 (m, 3 H), 7.20 (d,  $J = 9.0$  Hz, 2 H), 6.98 (br s, 1 H), 6.76 (d,  $J = 9.0$  Hz, 2 H), 6.46 (d,  $J = 8.5$  Hz, 1 H), 4.34 (ABq,  $J = 19.0, 13.0$  Hz, 2 H), 3.73 (s, 3 H);  $^{13}\text{C}$  NMR (125 MHz,  $\text{CDCl}_3$ ): 167.9, 164.9, 156.4, 155.2, 137.2, 135.1, 131.3, 129.1, 128.9, 128.8, 128.6, 128.1, 127.1, 123.0, 114.4, 55.5, 50.7, 37.0; HRMS (ESI): calcd for  $\text{C}_{24}\text{H}_{22}\text{N}_4\text{O}_3\text{S}$  ( $\text{M} + \text{H}$ ) $^+$ , 447.1485; found, 447.1485.

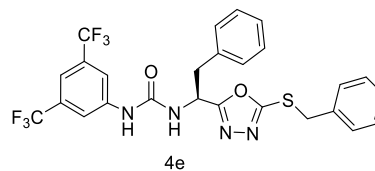
**1-((S)-5-(Benzylthio)-1,3,4-oxadiazol-2-yl)(phenyl)methyl)-3-(4-nitrophenyl)urea (4c).** White solid; yield = 160 mg (70%); mp 186–187 °C;  $[\alpha]_{\text{D}}^{25.8} = +28.2$  (c 0.96,  $\text{EtOAc}$ ); IR (neat)  $\nu_{\text{max}}$   $\text{cm}^{-1}$ : 1603



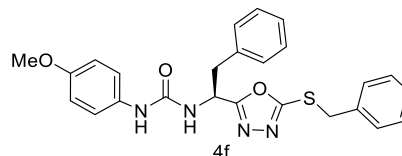
(C=N), 1699 (C=O), 3363;  $^1\text{H}$  NMR (200 MHz, DMSO): 9.52 (s, 1 H), 8.60 (d,  $J = 3.6$  Hz, 2 H), 8.18 (d,  $J = 3.6$  Hz, 2 H), 7.94 (d,  $J = 3.0$  Hz, 2 H), 7.89–7.83 (m, 5 H), 7.75–7.70 (m, 2 H), 6.83–6.82 (m, 1 H), 4.94, 4.92 (ABq,  $J = 5.6$  Hz, 2 H).  $^{13}\text{C}$  NMR (50 MHz, DMSO): 167.6, 164.1, 154.0, 146.7, 141.5, 137.2, 136.9, 129.5, 129.4, 129.1, 129.0, 128.2, 127.8, 125.6, 117.7, 50.4, 36.4; HRMS (ESI): calcd for  $\text{C}_{23}\text{H}_{19}\text{N}_5\text{O}_4\text{S}$  ( $\text{M} + \text{H}$ ) $^+$ , 462.1230; found, 462.1230.



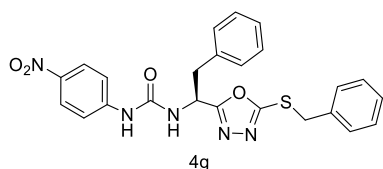
**1-((S)-5-(Benzylthio)-1,3,4-oxadiazol-2-yl)(phenyl)methyl)-3-p-tolylurea (4d).** White solid; yield = 125 mg (58%); mp 118.1–119.0 °C;  $[\alpha]_{\text{D}}^{25} = -16.5$  (c 1.05,  $\text{CHCl}_3$ ); IR (neat)  $\nu_{\text{max}}$   $\text{cm}^{-1}$ : 1592 (C=N), 1638 (C=O), 3300;  $^1\text{H}$  NMR (200 MHz,  $\text{CDCl}_3$ ): 8.06 (s, 1 H), 7.31–7.29 (m, 10 H), 7.23 (d,  $J = 8.4$  Hz, 2 H), 7.02 (d,  $J = 8.4$  Hz, 2 H), 6.53–6.48 (m, 1 H), 4.37 (s, 2 H), 2.28 (s, 3 H);  $^{13}\text{C}$  NMR (50 MHz,  $\text{CDCl}_3$ ): 168.1, 165.0, 155.0, 137.2, 136.1, 134.9, 132.8, 129.5, 129.1, 129.0, 128.9, 128.6, 128.2, 127.1, 120.3, 50.5, 37.0, 20.8; HRMS (ESI): calcd for  $\text{C}_{24}\text{H}_{22}\text{N}_4\text{O}_2\text{S}$  ( $\text{M} + \text{H}$ ) $^+$ , 431.1563; found, 431.1536.



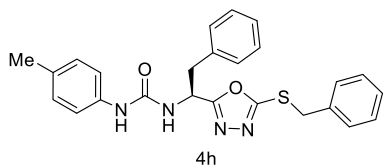
**1-(3,5-Bis(trifluoromethyl)phenyl)-3-((S)-5-(benzylthio)-1,3,4-oxadiazol-2-yl)-2-phenylethyl)urea (4e).** Colorless crystal; yield = 220 mg (78%); mp 167–168 °C;  $[\alpha]_{\text{D}}^{25} = -53.0$  (c 1.01,  $\text{CHCl}_3$ ); IR (neat)  $\nu_{\text{max}}$   $\text{cm}^{-1}$ : 1581 (C=N), 1658 (C=O), 3304;  $^1\text{H}$  NMR (500 MHz,  $\text{CDCl}_3$ ): 8.48 (s, 1 H), 7.75 (s, 2 H), 7.37 (t,  $J = 7.5$  Hz, 3 H), 7.34–7.26 (m, 3 H), 7.18 (br s, 3 H), 6.96 (d,  $J = 4.0$  Hz, 2 H), 6.85 (d,  $J = 8.5$  Hz, 1 H), 5.6–5.5 (m, 1 H), 4.41 (ABq,  $J = 17.5, 13.0$  Hz, 2 H), 3.05 (dd,  $J = 13.5, 6.0$  Hz, 1 H), 2.87 (dd,  $J = 13.5, 6.0$  Hz, 1 H);  $^{13}\text{C}$  NMR (125 MHz,  $\text{CDCl}_3$ ): 169.1, 165.4, 153.9, 140.7, 134.8, 134.7, 131.8 (q,  $J = 29.7$  Hz), 129.3, 129.0, 128.9, 128.7, 128.5, 127.5, 123.2 (q,  $J = 269.0$  Hz), 118.0, 115.5, 47.8, 40.2, 37.0; HRMS (ESI): calcd for  $\text{C}_{26}\text{H}_{20}\text{F}_6\text{N}_4\text{O}_2\text{S}$  ( $\text{M} + \text{H}$ ) $^+$ , 567.1283; found, 567.1284.



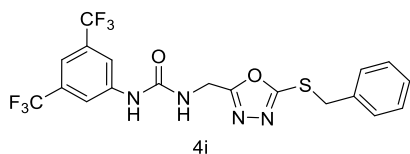
**1-((S)-5-(Benzylthio)-1,3,4-oxadiazol-2-yl)-2-phenylethyl)-3-(4-methoxyphenyl)urea (4f).** White solid; yield = 126 mg (55%); mp 163–164 °C;  $[\alpha]_{\text{D}}^{25.1} = -17.05$  (c 1.33,  $\text{CHCl}_3$ ); IR (neat)  $\nu_{\text{max}}$   $\text{cm}^{-1}$ : 1631 (C=N), 1660 (C=O), 3334;  $^1\text{H}$  NMR (500 MHz,  $\text{CDCl}_3$ ): 7.37 (d,  $J = 7$  Hz, 2 H), 7.33–7.27 (m, 3 H), 7.20–7.17 (m, 4 H), 7.12 (d,  $J = 9$  Hz, 2 H), 7.02–7.00 (m, 2 H), 6.77 (d,  $J = 9.0$  Hz, 2 H), 6.04 (d,  $J = 6.5$  Hz, 1 H), 5.53 (dd,  $J = 15.0, 6.5$  Hz, 1 H), 4.4–4.36 (m, 2 H), 3.76 (s, 3 H), 3.15 (dd,  $J = 14.0, 6.5$  Hz, 1 H), 3.06 (dd,  $J = 14.0, 6.5$  Hz, 1 H).  $^{13}\text{C}$  NMR (125 MHz,  $\text{CDCl}_3$ ): 168.2, 164.5, 156.8, 155.3, 135.4, 135.3, 130.9, 129.4, 129.0, 128.8, 128.6, 128.2, 127.2, 123.8, 114.5, 55.5, 47.9, 40.0, 36.9; HRMS (ESI): calcd for  $\text{C}_{25}\text{H}_{24}\text{N}_4\text{O}_3\text{S}$  ( $\text{M} + \text{H}$ ) $^+$ , 461.1641; found, 461.1642.



1-((S)-1-(5-(Benzylthio)-1,3,4-oxadiazol-2-yl)-2-phenylethyl)-3-(4-nitrophenyl)urea (**4g**). White solid; yield = 171 mg (72%); mp 190–192 °C;  $[\alpha]_D^{25.2} = -23.3$  (c 1.04, EtOAc); IR (neat)  $\nu_{\max}$   $\text{cm}^{-1}$ : 1608 (C=N), 1676 (C=O), 3350;  $^1\text{H NMR}$  (200 MHz, DMSO): 9.40 (s, 1H), 8.13 (d,  $J = 9.2$  Hz, 2 H), 7.58 (d,  $J = 9.2$  Hz, 2 H), 7.44–7.39 (m, 2 H), 7.35–7.16 (m, 9 H), 5.33–5.25 (m, 1 H), 4.46 (s, 2 H), 3.28–3.10 (m, 2H);  $^{13}\text{C NMR}$  (50 MHz, DMSO): 168.1, 163.6, 154.2, 146.9, 141.3, 137.0, 136.8, 129.7, 129.4, 129.0, 128.9, 128.2, 127.3, 125.6, 117.7, 47.8, 38.3, 36.3; HRMS (ESI): calcd for  $\text{C}_{24}\text{H}_{21}\text{N}_5\text{O}_4\text{S}$  ( $\text{M} + \text{H}$ )<sup>+</sup>, 476.1387; found, 476.1385.



1-((S)-1-(5-(Benzylthio)-1,3,4-oxadiazol-2-yl)-2-phenylethyl)-3-(4-methylphenyl)urea (**4h**). White solid; yield = 133 mg (60%); mp 165–166 °C;  $[\alpha]_D^{24.9} = -26.1$  (c 1.04,  $\text{CHCl}_3$ ); IR (neat)  $\nu_{\max}$   $\text{cm}^{-1}$ : 1593 (C=N), 1665 (C=O), 3347;  $^1\text{H NMR}$  (200 MHz,  $\text{CDCl}_3$ ): 7.36–7.35 (m, 3 H), 7.32–7.28 (m, 3 H), 7.19–7.18 (m, 3 H), 7.12 (d,  $J = 3.2$  Hz, 2 H), 7.02–7.00 (m, 4 H), 6.21 (d,  $J = 3.6$  Hz, 1 H), 5.54 (dd,  $J = 2.8$  Hz, 1 H), 4.38, 4.35 (ABq,  $J = 5.2$  Hz, 2 H), 3.14 (dd,  $J = 5.6, 2.8$  Hz, 1 H), 3.06 (dd,  $J = 5.6, 2.8$  Hz, 1 H), 2.27 (s, 3 H);  $^{13}\text{C NMR}$  (50 MHz,  $\text{CDCl}_3$ ): 168.3, 164.5, 154.9, 135.8, 135.4, 135.2, 133.3, 129.6, 129.4, 129.0, 128.8, 128.6, 128.2, 127.2, 121.0, 47.9, 40.1, 36.9, 20.7; HRMS (ESI): calcd for  $\text{C}_{25}\text{H}_{24}\text{N}_4\text{O}_2\text{S}$  ( $\text{M} + \text{H}$ )<sup>+</sup>, 445.1692; found, 445.1693.



1-((S)-1-(5-(Benzylthio)-1,3,4-oxadiazol-2-yl)methyl)urea (**4i**). White solid; yield = 161 mg (68%); mp 180.1–180.9 °C; IR (neat)  $\nu_{\max}$   $\text{cm}^{-1}$ : 1625 (C=N), 1658 (C=O), 3365;  $^1\text{H NMR}$  (500 MHz,  $\text{CDCl}_3$ ): 8.66 (s, 1 H), 7.83 (br s, 2 H), 7.38 (s, 1 H), 7.30–7.27 (m, 2 H), 7.25–7.22 (2 H), 4.69 (s, 2 H), 4.36 (s, 2 H);  $^{13}\text{C NMR}$  (125 MHz,  $\text{CDCl}_3$ ): 166.7, 166.1, 154.7, 140.5, 134.2, 131.9 (q,  $J = 32.5$  Hz), 128.9, 128.9, 128.4, 123.1 (q,  $J = 271.3$  Hz), 118.1, 115.8, 36.9, 35.4; HRMS (ESI): calcd for  $\text{C}_{19}\text{H}_{14}\text{F}_6\text{N}_4\text{O}_2\text{S}$  ( $\text{M} + \text{H}$ )<sup>+</sup>, 477.0814; found, 477.0812.

**Biological Studies. Materials.** All chemicals were procured from Sigma chemicals (St. Louis, MO), unless specified. Dulbecco's modified Eagle's medium (DMEM), fetal bovine serum (FBS) from Gibco Life Technologies (Carlsbad, CA). Lipofectamine, secondary antibodies tagged with Alexa fluor, and Prolong Diamond anti-fade reagent were from Invitrogen (Carlsbad, CA). Following antibodies were used in the current study: for RECQL1 (#A300-450A, Bethyl), BLM (#sc-365753, SCBT), WRN (#A300-238A Bethyl), RECQL5 (#sc-515150, SCBT; #5847S, CST),  $\gamma$ -H2AX (#H-5912, Sigma), H2AX (#SAB4501369, Sigma), RPA32 (#A300-244a, Bethyl), Ku 80 (#2180, CST), DNA-PKc (# 4602, CST), p-MRE11 (#8344, CST), MRE11 (# 8344, CST), p-NBS1 (#8344, CST), NBS1 (#8344, CST), RADS0 (#GTX70228, Genetex; #8344, CST), RAD51 (#sc-8349, SCBT; #PC 130, Sigma), ATM (#sc23921, SCBT), p-ATM (#5883, CST), ATR (Calbiochem, #PC 538), p-ATR (#2853, CST), CHK2 (#sc17748, SCBT), p-CHK2 (#2197, CST), CHK1 (sc-8408 SCBT), p-CHK1 (#2348, CST), p-p53 (#9286, CST), FLAG (#F3165,

Sigma),  $\beta$ -actin (#ab228001, #ab8227, Abcam),  $\alpha$ -tubulin (#T6199, Sigma) and anti-FLAG M2 magnetic beads (#M8823, Sigma). Following western blotting material used in the study: Lumi-Light Plus western blotting kit (Roche Applied Science, Baden-Wuerttemberg, Mannheim) and nitrocellulose membrane (Pall Life Sciences, Easthills, NY).

**Cell Culture.** U2-OS cell line was procured from American Type Culture Collection, MCF-7, T47D, and MDA-MB-231 cells were purchased from European Collection of Authenticated Cell Cultures. The cells were cultured in DMEM medium supplemented with FBS (10%), penicillin (100 U/mL), and streptomycin (100  $\mu\text{g}/\text{mL}$ ). The cells were grown in an incubator (37 °C, 5%  $\text{CO}_2$ ).

**MTT Assay for Cell Viability.** Cells ( $4 \times 10^3$  cells/well) were seeded in 96-well plates and allowed to grow overnight. The cells were treated with the vehicle [ $<0.1\%$  dimethyl sulfoxide (DMSO)] or various concentrations of test compounds for 72 h. 3-(4,5-Dimethylthiazol-2-yl)-2,5-diphenyltetrazolium bromide (MTT) solution (0.5 mg/mL) was added for 6 h. The formazan crystals in the viable cells were solubilized with 0.01 N HCl (100  $\mu\text{L}$ ) with 10% sodium dodecyl sulphate (SDS) and the absorbance was read at 550 nm in a multiplate reader.

**Clonogenic Survival Assay.** The cells (500/well) were seeded in 6-well plates and allowed to grow overnight. The cells were incubated with the vehicle (0.1% DMSO) or different concentrations of test compounds for 8–10 days in the complete growth media. The colonies were fixed with methanol and stained with 0.5% crystal violet in 1:1 methanol–water. The colonies were counted, and images of the colonies scanned. The surviving fractions were determined from the colony counts after correcting for the plating efficiency of the nontreated controls.

**Cell Cycle and Sub-G1 Analyses by Flow Cytometry.** The assay was carried out following a reported method with minor modifications.<sup>40</sup> The cells ( $1 \times 10^5$  cells/well), grown overnight, were treated with **4a** for the indicated time period. Cells were washed with cold phosphate-buffered saline (PBS), trypsinized, and incubated in hypotonic buffer (0.1% sodium citrate, 0.1% Triton X-100) containing propidium iodide (400  $\mu\text{g}/\text{mL}$ ) and RNase A (200  $\mu\text{g}/\text{mL}$ ) for 30 min. Further, cells (at least  $2 \times 10^4$ ) were acquired with a Partec CyFlo flow cytometer. Flow cytometer data were analyzed by FlowJo software.

**Cell Lysate Preparations and Immunoblot Assay.** After indicated treatments, cells were lysed in a lysis buffer [Tris (20 mM, pH 7.4), NaCl (250 mM), ethylenediaminetetraacetic acid (EDTA) (2 mM pH 8.0), Triton X-100 (0.5%), aprotinin (0.01  $\mu\text{g}/\text{mL}$ ), leupeptin (0.01  $\mu\text{g}/\text{mL}$ ), PMSF (0.4 mM), and  $\text{Na}_3\text{VO}_4$  (4 mM)]. The lysates were centrifuged (16,500g, 10 min) and the supernatants were collected to obtain the whole cell extracts. Different cell fractions were isolated after following a reported protocol.<sup>41</sup> Briefly, control and treated cells were lysed in buffer A [HEPES (10 mM, pH 7.9), glycerol (10%), sucrose (0.34 M) KCl,  $\text{MgCl}_2$  (1.5 mM), EDTA (0.2 mM), Triton X-100 (0.1%), and protease inhibitor cock-tail. After 20 min incubation, samples were centrifuged (4 min, 1300g, 4 °C) to obtain the nuclear pellet. Nuclei were washed once in buffer A, and then lysed in buffer B [EDTA (3 mM), ethylene glycol tetraacetic acid (EGTA) (0.2 mM), dithiothreitol (1 mM), and protease inhibitors cock-tail. The lysate was centrifuged (4 min, 1700g, 4 °C). The supernatant was considered as soluble nuclear fractions (F2) while pellet contains insoluble chromatin fraction (F3). This chromatin pellet (F3) was washed once with buffer B and suspended in buffer A plus  $\text{CaCl}_2$  (1 mM) and micrococcal nuclease (0.2 U, Sigma). After incubation at 37 °C for 5 min, the nuclease reaction was stopped by the addition of 1 mM EGTA, and the lysate was considered as a chromatin fraction (F4). For the total nuclear fraction, F2 and F4 were pooled together. The cell lysates were separated by 8–15% SDS-polyacrylamide gel electrophoresis and transferred to a nitrocellulose membrane. The membranes were blocked for 1 h at room temperature in TBST buffer [Tris–HCl (20 mM) pH 7.6, NaCl (137 mM), and Tween-20 (0.1%)] containing 5% (w/v) nonfat milk and incubated overnight at 4 °C with their respective specific primary antibodies. After several washes, suitable horseradish peroxidase-

conjugated secondary antibodies were added, the membranes were incubated further for 2 h, and the blots were developed using a Lumi-Light Plus western blotting kit. Protein bands detected using Syngene GBox XX6 and GeneSys software and the intensity ratios of immunoblots to that of normal control, taken as 1 (arbitrary unit) were quantified after normalizing with respect to the loading controls.

**Knockout, Knockdown, and Ectopic Expression.** All the CRISPR-CAS9 double nickase plasmids (Control and RECQL5) and lentivirus-expressing shRNA (control, RECQL1, RECQL5, WRN, and BLM) were purchased from Santa Cruz Biotechnology (Dallas, TX, USA). Exponentially growing MCF-7 cells were transfected using lipofectamine 3000 and CRISPR-CAS9 plasmids. For knockdown, exponentially growing MCF-7/U2-OS cells were treated with lentivirus (control, RECQL1, RECQL5, WRN, or BLM shRNA) and polybrene (20  $\mu\text{g}/\text{mL}$ ). Further, cells were selected in the presence of puromycin (1  $\mu\text{g}/\text{mL}$ ) and stable knockout and knockdown efficiency was assessed by western blotting. For ectopic expression, exponentially growing cells were transiently transfected with EVs, RECQL5 wildtype, and mutant protein expressing plasmids by the standard calcium phosphate method for 16 h, and cells were allowed to grow for another 4 h in complete growth medium. Ectopic expression was assessed by western blotting or fluorescence microscopy.

**Immunoprecipitation.** Respective RECQL5-KO cells ( $1 \times 10^7$  cells) were transfected with EVs and RECQL5 (WT)-FLAG by calcium phosphate method as mentioned above. After treatment, chromatin fractions were prepared as mentioned above. Further, chromatin extracts (1 mg) were subjected to immunoprecipitation (IP) with anti-FLAG M2 magnetic beads, in the presence of EtBr (10  $\mu\text{g}/\text{mL}$ ), overnight under rotation (4  $^\circ\text{C}$ ). Beads were extensively washed with lysis buffer. Input and IP lysates were subjected to western blotting of RECQL5, FLAG, and RAD51 proteins.

**Immunofluorescence Staining and Microscopy.** Cells ( $7.5 \times 10^4$  cells/well) were seeded in a 6-well plate containing glass cover slips. Cells were treated for the indicated time, washed with PBS, and fixed by chilled methanol. The fixed cells were washed twice with PBS and permeabilized with PBST (0.1% Tween 20) for about 10 min. Further, the cells were blocked with 5% bovine serum albumin (BSA) for 2 h, incubated with the respective primary antibodies (1:6000, 2.5% BSA) overnight (4  $^\circ\text{C}$ ). After washing with PBST, secondary antibodies tagged with Alexa Fluor-488/Alexa Fluor-594 with suitable isotype controls (1:2000, 2.5% BSA) were added (3 h, RT). Cells were washed twice with PBST, coverslips were dried and mounted on slides with Prolong Diamond anti-fade reagent (containing DAPI). Mounted slides were then analyzed with a confocal microscope (LSM 780, Carl Zeiss, Germany). Image analysis was performed using Zeiss Zen software. Approximately 80–100 nuclei, in duplicates, were analyzed for each sample in 3–5 experiments.

**RECQL5 Cloning, Expression, and Purification.** Full length ORFs of RECQL5 (WT and K58M mutant) were obtained by PCR amplification from recombinant pCMV6-AN-His-DDK plasmid (#RC209460, Origene, USA) as the template using the primers 1 and 2 (Table S1). The PCR product was inserted in pET29 in the *NdeI* and *XhoI* sites. After verifying the construct, *E. coli* Rosetta-gami-2 cells were transformed with the recombinant plasmid. A batch culture (1000 mL) of these bacteria were induced with IPTG (300  $\mu\text{M}$ , 3 h, RT) and harvested. The cell pellet was resuspended in equilibration buffer A [Tris-HCl (25 mM, pH. 8), NaCl (300 mM),  $\text{MgCl}_2$  (2 mM),  $\beta$ -mercaptoethanol (BME) (2 mM), glycerol (3%), PMSF (2 mM), and protease inhibitor cocktail (Roche)]. After initial treatment with lysozyme (200  $\mu\text{g}/\text{mL}$ ) and benzonase (1 U) for 30 min, the suspension was sonicated for 5 min (30% amplitude; 4 s pulse). The cell lysate was centrifuged (8000g, 30 min) and the clear lysate was mixed with the pre-equilibrated Ni-NTA resin (0.5 mL, 30 min, 4  $^\circ\text{C}$ ; Qiagen) in a rotary mixer. The mixture was further loaded in a column and the resin was repeatedly washed equilibration buffer containing imidazole (30 mM). The bound protein was eluted from the column by repeated washing with equilibration buffer containing 300 mM imidazole ( $6 \times 0.5$  mL). Excess imidazole was removed using a PD10 desalting column. The protein was then concentrated

and equilibrated with buffer containing NaCl (600 mM, pH 7.6) and passed through a superdex 200 Gel Filtration column. The fraction eluting at  $\sim 80$ –120 kDa was collected, concentrated and equilibrated with buffer B [Tris-HCl (25 mM, pH. 7.6), NaCl (50 mM),  $\text{MgCl}_2$  (2 mM) BME (2 mM), glycerol (3%)]. Protein was characterized by western blotting with anti-HIS and anti-RECQL5.

**Generation of Mutants RECQL5 by Site-Directed Mutagenesis.** Full length ORF of RECQL5 with *EcoRI* and *KpnI* sites was obtained by PCR amplification from the recombinant pCMV6-AN-His-DDK plasmid, by using primer 3 and 4 (Table S1). The PCR product was inserted in a p3X FLAG-CMV7.1 vector. The fusion PCR protocol was used to generate the RECQL5 (F666A)-FLAG mutant. By using p3X-RECQL5-FLAG-CMV7.1 as a template, two sets of parallel PCR reactions were performed. One with primers 3 and 6 and other with primers 5 and 4 (Table S1). The amplified products (approx. 2 and 1 kb) were gel purified and PCR amplified with primers 3 and 4 to obtain the RECQL5 (F666A)-FLAG mutant product. This product was cloned in the p3X FLAG-CMV7.1 vector. The F666A mutation was confirmed by sequencing by using primers 7 and 8. For RECQL5-RFP, full length RECQL5 ORF from the pCMV6-AN-His-DDK plasmid was shuffled to the pCMV-AC-RFP vector (Origene, USA). Further, the helicase dead RECQL5 (K58M)-RFP mutant was obtained with primers 9 and 10 (Table S1), following QuikChange II XL Site-Directed Mutagenesis kit (#200521, Agilent, CA, USA).

**RECQL5 Helicase Assay.** The forked substrate for the helicase assay was prepared by annealing 5' FAM labeled oligo with its complementary 3' BHQ1 labeled oligo (equimolar 30 mer Oligo1 and 2, Table S1). The mixture was heated to 95  $^\circ\text{C}$  for 5 min and slowly cooled down to 25  $^\circ\text{C}$ . For the helicase assay, purified RECQL5 protein (20 nM; WT) was incubated with different concentrations of 4a in reaction buffer [Tris-HCl (10 mM, pH 8.0),  $\text{MgCl}_2$  (2 mM), glycerol (1%), and BSA (100  $\mu\text{g}/\text{mL}$ )] at 4  $^\circ\text{C}$  for 30 min. Finally, duplex forked DNA (20 nM) and ATP (2 mM) were added and the FAM fluorescence was measured in a fluorescence multiplate reader ( $\lambda_{\text{ex}}$ : 495 nm and  $\lambda_{\text{em}}$ : 520 nm) at different time points. Helicase activity of RECQL5-WT and RECQL5-K58M proteins was also compared by employing the above assay.

**DNA Binding Activity Assay.** Oligonucleotide strand (Oligo 3, 5 pmol) was radiolabeled with [ $\gamma^{32}\text{P}$ ] at its 5' end. Labeling was performed by incubating the oligo, ATP ( $\gamma^{32}\text{P}$ ; 3000 Ci/mmol), and polynucleotide kinase in polynucleotide kinase buffer (New England Biolabs, Inc). Labeled oligo was purified by G25 column (GE, USA). The linear dsDNA substrate was prepared by mixing equimolar oligo 3 (radio-labelled) and oligo 4 (Table S1) in TE buffer [Tris-HCl (10 mM, pH 7.6, 1 mM EDTA)], heating at 95  $^\circ\text{C}$  for 5 min, and allowed slowly to cool down to 25  $^\circ\text{C}$ . The purified RECQL5 protein (50–200 nM) was incubated with 4a (0–10  $\mu\text{M}$ ) in buffer [Tris-HCl (10 mM, pH 7.6), NaCl (50 mM), KCl (25 mM), BSA (100  $\mu\text{g}/\text{mL}$ ), and BME (2 mM)] for 30 min. Further, the dsDNA substrate was added and incubated for additional 15 min. The products were resolved on 6% native-polyacrylamide gel made with TBE (0.5 $\times$ ) and KCl (50 mM) by electrophoresis in 0.5 $\times$  TBE containing KCl (50 mM). The gels were then dried and the autoradiograms were developed on a X-ray film.

**RECQL5 ATPase Assay.** ATP consumption by RECQL5 ATPase activity was assessed by an ATP determination kit (#A22066, Thermo Scientific). Briefly, purified RECQL5 protein (200 nM) was incubated with 4a (0.1–10  $\mu\text{M}$ ) for 60 min in reaction buffer [Tris-HCl (10 mM, pH. 7.4), BSA (0.1%)] at 4  $^\circ\text{C}$ . Further, forked dsDNA (50 nM), luciferin, and luciferase were added to the reaction mixture for 15 min. Finally, ATP (2 mM) was added for 1 h and read at 560 nm in a multiplate fluorescence reader.

**Development of Cisplatin-Resistant Breast Cancer Cells.** This was developed as per the reported protocol.<sup>29</sup> The MCF-7 cells, seeded at 70–80% confluence for 16 h in a T-25 flask, were treated with a high CDDP concentration (10  $\mu\text{M}$ ) for 2 days. After 2 days, cells were washed and allowed to grow in CDDP free regular medium for another 2 days. The above procedure was repeated for 4–6 weeks and cells were analyzed for cell survival by the MTT assay. CDDP-resistant MCF-7 cells were named MCF-7<sup>CDDP</sup> cells.

#### 4a Treatment in the Xenograft Tumor Model in NUDE Mice.

Female NUDE mice (approx. 8 weeks) were procured from Advanced Centre for Treatment, Research, and Education in Cancer (ACTREC, Navi Mumbai, India). The due approval for the use of animals for the current study was obtained from the Institutional Animal Ethics Committee (IAEC) of Bhabha Atomic Research Center (Approval number BAEC/16/16). Institutional guidelines were strictly adhered for housing mice in standard individually ventilated cages, diet, water, dark light cycle, and experimental protocol. Exponentially growing RECQL5-WT MCF-7 and RECQL5-KO MCF-7 cells ( $1 \times 10^7$  cells/100  $\mu$ L DMEM) were injected into the right flank of the mice. Subcutaneous injection of  $\beta$ -estradiol (200 ng/0.1 mL PBS) was given on alternate days. After 15 days of injection, mice bearing palpable RECQL5-WT and RECQL5-KO tumors were randomized into four different groups ( $n = 8$ ), for example, (1) RECQL5-WT (vehicle 100  $\mu$ L), (2) RECQL5-WT (4a 50 mg/kg/day; 100  $\mu$ L), (3) RECQL5-KO (vehicle 100  $\mu$ L), and (4) RECQL5-KO (4a 50 mg/kg/day; 100  $\mu$ L). 4a was prepared in 0.5% DMSO in Neobee M5 oil (Sigma). The above formulation was given through oral gavage on every alternate day for 30 days. TV was evaluated by measuring the perpendicular diameter axes of the tumor with vernier calipers (axes labels-“a”, long axis, and “b”, short axis).<sup>37</sup> Experiments were blinded by allowing two independent groups to deliver the formulation and measure the TV of the coded groups of mice. The body weight of animals was assessed regularly. At the end of the whole experiment, mice were sacrificed by euthanizing the animals by CO<sub>2</sub> asphyxiation in compliance with the standard procedure approved by the IAEC. Briefly, CO<sub>2</sub> cages were used to steadily replace the air with CO<sub>2</sub> (5–20% cage air with CO<sub>2</sub> per minute) for 8 min. After CO<sub>2</sub> treatment, mice were returned to ambient air for 15 min to ensure no recovery. Tumors were excised, weighed, and photographed. The inspection of major morphological changes of organs was also carried out.

**Toxicity Studies in the Preclinical Mouse Model.** Mice (20–25 gm, male C15BL16 strain, approval no. BAEC/10/16) were obtained from the BARC animal breeding facility. Guidelines for animal treatment and maintenance were followed as mentioned above. Mice were given a single oral gavage of the vehicle or 4a (100 mg/kg body wt;  $n = 8$  mice) and kept under observation for 30 days. Body weight, behavior, stool texture, and food and water intake was monitored every alternate days. After 30 days, animals were sacrificed, as mentioned above, and blood and spleen were collected. The blood serum was subjected to the biochemical analysis of creatinine (mg/dL), ALP (U/L), and SGPT (U/L) with an auto analyzer (Rx Daytona, Randox, crumlin county, Antrim, UK). Total cells from the spleen were removed as per the reported protocol.<sup>42</sup>

**HPLC Analysis of 4a Concentrations in the Serum.** Nude mice were given oral gavage of vehicle or 4a (50 mg/kg body wt  $n = 3$ ). The blood was collected immediately after sacrificing mice at different time points. Serum samples (100  $\mu$ L) were mixed with the solvent mixture {methanol: acetonitrile (ACN) (70:30); 200  $\mu$ L to precipitate proteins. The serum and solvent mixture was intermittently vortexed at the interval of 5 min for 30 min. The mixture was centrifuged (12,000g; 10 min). Solvent extraction was repeated once again with the above process. The clear supernatant, obtained from the above protocol, was subjected to HPLC analysis. HPLC instrument (model 2200, Jasco, Japan) with following parameters were used for the analysis: eluent (ACN/water - 70:30), flow rate (1 mL/min), Eurospher 100 C18, 7  $\mu$ m column (25 mm  $\times$  4.6 mm i.d.; Knauer GmbH, Berlin, Germany), and UV detection (254 nm). The 4a concentration was measured using a standard curve of 4a. The calibration curve was found to be linear over the concentration range of 10–2000 nM. To obtain the serum concentration of 4a, dilution factor used during the solvent extraction was adjusted.

**In Silico Docking Study.** The crystal structure of human RECQL5 complexed with ADP (PDB ID: 5LB3) was downloaded from the Protein Data Bank (<https://www.rcsb.org/>) and used for molecular docking. ADP was used as a reference ligand and protein hydrogens and charges were added at pH 7, using LeadIT module in BioSolveIT software suite [LeadIT version 2.3.2; BioSolveIT GmbH, Sankt Augustin, Germany, 2019, [www.biosolveit.de/LeadIT](http://www.biosolveit.de/LeadIT)]. The com-

pounds were docked into the solvent accessible ATP binding pocket of RECQL5 helicase using LeadIT with a limit of 200 poses per compound. The binding pocket was defined around the ADP molecule within 10 Å limit. The molecule ranking was done using the FlexX scoring function. Top 10 docked poses per compound were listed and scored, and the binding free energy ( $\Delta G$ ) was obtained for the best pose. The docked compounds were visually inspected for H-bonds, VDW clashes, and electrostatic and hydrophobic interactions. The co-crystallized ligand ADP lied close to the two molecules (figure of surface diagrams with ligands superposed). Important amino acid residues of helicase involved in the putative interactions with the ligands were shown in 2D interaction diagrams. The hydrogen bonding interactions were shown in dotted lines. Structural, surface, and superposition figures were made using the PyMOL Molecular Graphics System, Version 2.0 Schrödinger, LLC.

**Clinical Data Analysis.** Based on breast cancer database,<sup>17</sup> disease outcomes, that is, tumor-free survival, were assessed by using the online database ([www.kmplot.com](http://www.kmplot.com)).

**Statistical Analyses.** At least three independent experiments were carried out and values presented as mean  $\pm$  SEM or mean  $\pm$  SD. The statistical analysis was performed using GraphPad Prism 5.0. Two-tailed, unpaired, Student's *t*-test or ANOVA with Tukey post-hoc analysis was carried out, wherever necessary, to test the statistical significance of the data presented. A value of  $p < 0.05$  was considered significant. For animal experiments, all animal studies were conducted using eight animals per group for each experiment. The statistical significance was determined by using the Student's *t*-test.

## ■ ASSOCIATED CONTENT

### Supporting Information

The Supporting Information is available free of charge at <https://pubs.acs.org/doi/10.1021/acs.jmedchem.0c01692>.

Effect of compounds on cell viability and clonogenic potential; effects of 4a on different RECQL5-WT- and RECQL5-depleted breast cancer cells, DNA binding, and ATPase activity, role of 4a in DSB generation, apoptosis, NHEJ- and HRR-regulating proteins, stabilizing RECQL5-RAD51 complex, and cell cycle; pharmacokinetic and toxicity effects of 4a; HPLC purity; sequence of the primers and DNA oligos; NMR spectra; and oligonucleotides used in this study (PDF)

(PDB)

(PDB)

## ■ AUTHOR INFORMATION

### Corresponding Authors

Sunil Kumar Ghosh – Bio-Organic Division, Bhabha Atomic Research Centre, Mumbai 400085, India; Homi Bhabha National Institute, Mumbai 400094, India; [orcid.org/0000-0003-2508-6181](https://orcid.org/0000-0003-2508-6181); Email: [bisank@barc.gov.in](mailto:bisank@barc.gov.in)

Birija Sankar Patro – Bio-Organic Division, Bhabha Atomic Research Centre, Mumbai 400085, India; Homi Bhabha National Institute, Mumbai 400094, India; [orcid.org/0000-0001-9161-5913](https://orcid.org/0000-0001-9161-5913); Email: [ghsunil@barc.gov.in](mailto:ghsunil@barc.gov.in)

### Authors

Saikat Chakraborty – Bio-Organic Division, Bhabha Atomic Research Centre, Mumbai 400085, India; Homi Bhabha National Institute, Mumbai 400094, India

Kartik Dutta – Bio-Organic Division, Bhabha Atomic Research Centre, Mumbai 400085, India; Homi Bhabha National Institute, Mumbai 400094, India

Pooja Gupta – Bio-Organic Division, Bhabha Atomic Research Centre, Mumbai 400085, India; Homi Bhabha National Institute, Mumbai 400094, India

Anubrata Das – Bio-Organic Division, Bhabha Atomic Research Centre, Mumbai 400085, India; Homi Bhabha National Institute, Mumbai 400094, India

Amit Das – Homi Bhabha National Institute, Mumbai 400094, India; Radiation Biology & Health Sciences Division, Bhabha Atomic Research Centre, Mumbai 400085, India

Complete contact information is available at:  
<https://pubs.acs.org/10.1021/acs.jmedchem.0c01692>

### Author Contributions

S.C. and B.S.P. designed the biology experiments while K.D. and S.K.G. designed the chemistry experiments. S.C., P.G., and A.D. performed the biology experiments. K.D. synthesized and characterized the compounds. A.D. performed docking analyses. S.C., K.D., S.K.G., and B.S.P. contributed to data analysis, manuscript writing, and editing.

### Funding

This work was supported financially by the internal funding of the Bhabha Atomic Research Centre, Department of Atomic Energy, India.

### Notes

The authors declare no competing financial interest.

## ACKNOWLEDGMENTS

The authors would like to acknowledge the central animal house facility at the Bhabha Atomic Research Centre, Mumbai. The authors also like to acknowledge Ganesh Pai, and Ananda Guha Majumdar for their help in animal experimentation and protein purification, Raghunath Chowdhury and Binita Kishore Kumar for their help in HPLC analyses, respectively.

## REFERENCES

- (1) Bray, F.; Ferlay, J.; Soerjomataram, I.; Siegel, R. L.; Torre, L. A.; Jemal, A. Global Cancer Statistics 2018: GLOBOCAN Estimates of Incidence and Mortality Worldwide for 36 Cancers in 185 Countries. *Ca-Cancer J. Clin.* **2018**, *68*, 394–424.
- (2) Forouzanfar, M. H.; Foreman, K. J.; Delossantos, A. M.; Lozano, R.; Lopez, A. D.; Murray, C. J. L.; Naghavi, M. Breast and Cervical Cancer in 187 Countries between 1980 and 2010: A Systematic Analysis. *Lancet* **2011**, *378*, 1461–1484.
- (3) Waks, A. G.; Winer, E. P. Breast Cancer Treatment: A Review. *JAMA* **2019**, *321*, 288.
- (4) Wang, X.; Shi, Y.; Huang, D.; Guan, X. Emerging Therapeutic Modalities of PARP Inhibitors in Breast Cancer. *Cancer Treat. Rev.* **2018**, *68*, 62–68.
- (5) Exman, P.; Barroso-Sousa, R.; Tolaney, S. M. Evidence to Date: Talazoparib in the Treatment of Breast Cancer. *OncoTargets Ther.* **2019**, *12*, 5177–5187.
- (6) Popuri, V.; Tadokoro, T.; Croteau, D. L.; Bohr, V. A. Human RECQL5: Guarding the Crossroads of DNA Replication and Transcription and Providing Backup Capability. *Crit. Rev. Biochem. Mol. Biol.* **2013**, *48*, 289–299.
- (7) Brosh, R. M. DNA Helicases Involved in DNA Repair and Their Roles in Cancer. *Nat. Rev. Cancer* **2013**, *13*, 542–558.
- (8) Zhi, L.-Q.; Ma, W.; Zhang, H.; Zeng, S.-X.; Chen, B. Association of RECQL5 Gene Polymorphisms and Osteosarcoma in a Chinese Han Population. *Tumor Biol.* **2014**, *35*, 3255–3259.
- (9) Dong, Y. Z.; Huang, Y. X.; Lu, T. Single Nucleotide Polymorphism in the RECQL5 Gene Increased Osteosarcoma Susceptibility in a Chinese Han Population. *GMR, Genet. Mol. Res.* **2015**, *14*, 1899–1902.
- (10) Qi, Y.; Zhou, X. Haplotype Analysis of RECQL5 Gene and Laryngeal Cancer. *Tumor Biol.* **2014**, *35*, 2669–2673.

(11) He, Y.-J.; Qiao, Z.-Y.; Gao, B.; Zhang, X.-H.; Wen, Y.-Y. Association between RECQL5 Genetic Polymorphisms and Susceptibility to Breast Cancer. *Tumor Biol.* **2014**, *35*, 12201–12204.

(12) Arora, A.; Abdel-Fatah, T. M. A.; Agarwal, D.; Doherty, R.; Croteau, D. L.; Moseley, P. M.; Hameed, K.; Green, A.; Aleskandarany, M. A.; Rakha, E. A.; Patterson, K.; Ball, G.; Chan, S. Y. T.; Ellis, I. O.; Bohr, V. A.; Bryant, H. E.; Madhusudan, S. Clinicopathological and Prognostic Significance of RECQL5 Helicase Expression in Breast Cancers. *Carcinogenesis* **2016**, *37*, 63–71.

(13) Andrs, M.; Hasanova, Z.; Oravetzova, A.; Dobrovolna, J.; Janscak, P. RECQ5: A Mysterious Helicase at the Interface of DNA Replication and Transcription. *Genes* **2020**, *11*, 232.

(14) Schwendener, S.; Raynard, S.; Paliwal, S.; Cheng, A.; Kanagaraj, R.; Shevelev, I.; Stark, J. M.; Sung, P.; Janscak, P. Physical Interaction of RECQ5 Helicase with RAD51 Facilitates Its Anti-Recombinase Activity. *J. Biol. Chem.* **2010**, *285*, 15739–15745.

(15) Hosono, Y.; Abe, T.; Ishiai, M.; Islam, M. N.; Arakawa, H.; Wang, W.; Takeda, S.; Ishii, Y.; Takata, M.; Seki, M.; Enomoto, T. Tumor suppressor RecQL5 controls recombination induced by DNA crosslinking agents. *Biochim. Biophys. Acta, Mol. Cell Res.* **2014**, *1843*, 1002–1012.

(16) Roe, O. D.; Szulkin, A.; Anderssen, E.; Flatberg, A.; Sandeck, H.; Amundsen, T.; Erlandsen, S. E.; Dobra, K.; Sundstrom, S. H. Molecular Resistance Fingerprint of Pemetrexed and Platinum in a Long-Term Survivor of Mesothelioma. *PLoS One* **2012**, *7*, No. e40521.

(17) Györfy, B.; Lanczky, A.; Eklund, A. C.; Denkert, C.; Budczies, J.; Li, Q.; Szallasi, Z. An Online Survival Analysis Tool to Rapidly Assess the Effect of 22,277 Genes on Breast Cancer Prognosis Using Microarray Data of 1,809 Patients. *Breast Cancer Res. Treat.* **2010**, *123*, 725–731.

(18) Wang, Q.; Mgimpatsang, K. C.; Konstantinidou, M.; Shishkina, S. V.; Dömling, A. 1,3,4-Oxadiazoles by Ugi-Tetrazole and Huisgen Reaction. *Org. Lett.* **2019**, *21*, 7320–7323.

(19) Newman, J. A.; Aitkenhead, H.; Savitsky, P.; Gileadi, O. Insights into the RecQ Helicase Mechanism Revealed by the Structure of the Helicase Domain of Human RECQL5. *Nucleic Acids Res.* **2017**, *45*, 4231–4243.

(20) Gray, M. D.; Shen, J.-C.; Kamath-Loeb, A. S.; Blank, A.; Sopher, B. L.; Martin, G. M.; Oshima, J.; Loeb, L. A. The Werner syndrome protein is a DNA helicase. *Nat. Genet.* **1997**, *17*, 100–103.

(21) Garcia, P. L.; Liu, Y.; Jiricny, J.; West, S. C.; Janscak, P. Human RECQ5 $\beta$ , a protein with DNA helicase and strand-annealing activities in a single polypeptide. *EMBO J.* **2004**, *23*, 2882–2891.

(22) Aggarwal, M.; Sommers, J. A.; Shoemaker, R. H.; Brosh, R. M. Inhibition of Helicase Activity by a Small Molecule Impairs Werner Syndrome Helicase (WRN) Function in the Cellular Response to DNA Damage or Replication Stress. *Proc. Natl. Acad. Sci. U.S.A.* **2011**, *108*, 1525–1530.

(23) Tiwari, A.; Gopalan Kutty, N.; Kumar, N.; Chaudhary, A.; Vasanth Raj, P.; Shenoy, R.; Mallikarjuna Rao, C. Synthesis and Evaluation of Selected 1,3,4-Oxadiazole Derivatives for in Vitro Cytotoxicity and in Vivo Anti-Tumour Activity. *Cytotechnology* **2016**, *68*, 2553–2565.

(24) Hekal, M. H.; El-Naggar, A. M.; Abu El-Azm, F. S. M.; El-Sayed, W. M. Synthesis of New Oxadiazol-Phthalazinone Derivatives with Anti-Proliferative Activity; Molecular Docking, pro-Apoptotic, and Enzyme Inhibition Profile. *RSC Adv.* **2020**, *10*, 3675–3688.

(25) Hu, Y.; Lu, X.; Barnes, E.; Yan, M.; Lou, H.; Luo, G. Recq15 and Blm RecQ DNA Helicases Have Nonredundant Roles in Suppressing Crossovers. *Mol. Cell. Biol.* **2005**, *25*, 3431–3442.

(26) Hu, Y.; Raynard, S.; Sehorn, M. G.; Lu, X.; Bussen, W.; Zheng, L.; Stark, J. M.; Barnes, E. L.; Chi, P.; Janscak, P.; Jasin, M.; Vogel, H.; Sung, P.; Luo, G. RECQL5/Recq15 Helicase Regulates Homologous Recombination and Suppresses Tumour Formation via Disruption of Rad51 Presynaptic Filaments. *Genes Dev.* **2007**, *21*, 3073–3084.

(27) Paliwal, S.; Kanagaraj, R.; Sturzenegger, A.; Burdova, K.; Janscak, P. Human RECQ5 Helicase Promotes Repair of DNA

Double-Strand Breaks by Synthesis-Dependent Strand Annealing. *Nucleic Acids Res.* **2014**, *42*, 2380–2390.

(28) Islam, M. N.; Paquet, N.; Fox, D.; Dray, E.; Zheng, X.-F.; Klein, H.; Sung, P.; Wang, W. A Variant of the Breast Cancer Type 2 Susceptibility Protein (BRC) Repeat Is Essential for the RECQL5 Helicase to Interact with RAD51 Recombinase for Genome Stabilization. *J. Biol. Chem.* **2012**, *287*, 23808–23818.

(29) Helleday, T. Homologous Recombination in Cancer Development, Treatment and Development of Drug Resistance. *Carcinogenesis* **2010**, *31*, 955–960.

(30) Hengel, S. R.; Spies, M. A.; Spies, M. Small-Molecule Inhibitors Targeting DNA Repair and DNA Repair Deficiency in Research and Cancer Therapy. *Cell Chem. Biol.* **2017**, *24*, 1101–1119.

(31) Tyagi, M.; Patro, B. S. Salinomycin Reduces Growth, Proliferation and Metastasis of Cisplatin Resistant Breast Cancer Cells via NF-KB Deregulation. *Toxicol. In Vitro* **2019**, *60*, 125–133.

(32) Sarbajna, S.; Davies, D.; West, S. C. Roles of SLX1-SLX4, MUS81-EME1, and GEN1 in Avoiding Genome Instability and Mitotic Catastrophe. *Genes Dev.* **2014**, *28*, 1124–1136.

(33) Krajewska, M.; Fehrmann, R. S. N.; de Vries, E. G. E.; van Vugt, M. A. T. M. Regulators of Homologous Recombination Repair as Novel Targets for Cancer Treatment. *Front. Genet.* **2015**, *6*, 96.

(34) Orbegoso, C.; Marquina, G.; George, A.; Banerjee, S. The Role of Cediranib in Ovarian Cancer. *Expert Opin. Pharmacother.* **2017**, *18*, 1637–1648.

(35) Kaplan, A. R.; Gueble, S. E.; Liu, Y.; Oeck, S.; Kim, H.; Yun, Z.; Glazer, P. M. Cediranib Suppresses Homology-Directed DNA Repair through down-Regulation of BRCA1/2 and RAD51. *Sci. Transl. Med.* **2019**, *11*, No. eaav4508.

(36) Bagnolini, G.; Milano, D.; Manerba, M.; Schipani, F.; Ortega, J. A.; Gioia, D.; Falchi, F.; Balboni, A.; Farabegoli, F.; De Franco, F.; Robertson, J.; Pellicciari, R.; Pallavicini, I.; Peri, S.; Minucci, S.; Giroto, S.; Di Stefano, G.; Roberti, M.; Cavalli, A. Synthetic Lethality in Pancreatic Cancer: Discovery of a New RAD51-BRCA2 Small Molecule Disruptor That Inhibits Homologous Recombination and Synergizes with Olaparib. *J. Med. Chem.* **2020**, *63*, 2588–2619.

(37) Nguyen, G. H.; Dexheimer, T. S.; Rosenthal, A. S.; Chu, W. K.; Singh, D. K.; Mosedale, G.; Bachrati, C. Z.; Schultz, L.; Sakurai, M.; Savitsky, P.; Abu, M.; McHugh, P. J.; Bohr, V. A.; Harris, C. C.; Jadhav, A.; Gileadi, O.; Maloney, D. J.; Simeonov, A.; Hickson, I. D. A Small Molecule Inhibitor of the BLM Helicase Modulates Chromosome Stability in Human Cells. *Chem. Biol.* **2013**, *20*, 55–62.

(38) Yin, Q.-K.; Wang, C.-X.; Wang, Y.-Q.; Guo, Q.-L.; Zhang, Z.-L.; Ou, T.-M.; Huang, S.-L.; Li, D.; Wang, H.-G.; Tan, J.-H.; Chen, S.-B.; Huang, Z.-S. Discovery of Isaindigotone Derivatives as Novel Bloom's Syndrome Protein (BLM) Helicase Inhibitors That Disrupt the BLM/DNA Interactions and Regulate the Homologous Recombination Repair. *J. Med. Chem.* **2019**, *62*, 3147–3162.

(39) Islam, M. N.; Fox, D.; Guo, R.; Enomoto, T.; Wang, W. RecQL5 Promotes Genome Stabilization through Two Parallel Mechanisms-Interacting with RNA Polymerase II and Acting as a Helicase. *Mol. Cell. Biol.* **2010**, *30*, 2460–2472.

(40) Saha, B.; Patro, B. S.; Koli, M.; Pai, G.; Ray, J.; Bandyopadhyay, S. K.; Chattopadhyay, S. trans-4,4'-Dihydroxystilbene (DHS) inhibits human neuroblastoma tumor growth and induces mitochondrial and lysosomal damages in neuroblastoma cell lines. *Oncotarget* **2017**, *8*, 73905–73924.

(41) Patro, B. S.; Frohlich, R.; Bohr, V. A.; Stevnsner, T. WRN Helicase Regulates the ATR-CHEK1-Induced S-Phase Checkpoint Pathway in Response to Topoisomerase-I-DNA Covalent Complexes. *J. Cell Sci.* **2011**, *124*, 3967–3979.

(42) Han, L.; Meng, M.; Guo, M.; Cheng, D.; Shi, L.; Wang, X.; Wang, C. Immunomodulatory Activity of a Water-Soluble Polysaccharide Obtained from Highland Barley on Immunosuppressive Mice Models. *Food Funct.* **2019**, *10*, 304–314.